

STANDING SAUSAGE PERTURBATIONS IN SOLAR CORONAL SLABS WITH CONTINUOUS TRANSVERSE DENSITY PROFILES: CUTOFF WAVENUMBERS, EVANESCENT EIGENMODES, AND OSCILLATORY CONTINUUM

ZEXING WANG,¹ BO LI,¹ SHAO-XIA CHEN,¹ AND MIJIE SHI¹

¹*Shandong Provincial Key Laboratory of Optical Astronomy and Solar-Terrestrial Environment, Institute of Space Sciences, Shandong University, Weihai 264209, China*

Submitted to ApJ

ABSTRACT

The lack of observed sausage perturbations in solar active region loops is customarily attributed to the relevance of cutoff axial wavenumbers and the consequent absence of trapped modes (called “evanescent eigenmodes” here). However, some recent eigenvalue problem studies yield that cutoff wavenumbers may disappear for those equilibria where the external density varies sufficiently slowly, thereby casting doubt on the rarity of candidate sausage perturbations. We examine the responses of straight, transversely structured, coronal slabs to small-amplitude sausage-type perturbations that excite axial fundamentals by solving the pertinent initial value problem with eigensolutions for a closed domain. The density variation in the slab exterior is dictated by some steepness parameter μ , and cutoff wavenumbers are theoretically expected to be present (absent) when $\mu \geq 2$ ($\mu < 2$). However, our numerical results show no qualitative difference in the system evolution when μ varies, despite the differences in the modal behavior. Only oscillatory eigenmodes are permitted when $\mu \geq 2$. Our discrete eigenspectrum becomes increasingly closely spaced when the domain broadens, and an oscillatory continuum results for a truly open system. Oscillatory eigenmodes remain allowed and dominate the system evolution when $\mu < 2$. We show that the irrelevance of cutoff wavenumbers does not mean that all fast waves are evanescent. Rather, it means that an increasing number of evanescent eigenmodes emerge when the domain size increases. We conclude that sausage perturbations remain difficult to detect even for the waveguide formulated here.

Keywords: magnetohydrodynamics (MHD) — Sun: corona — Sun: magnetic fields — waves

1. INTRODUCTION

Solar coronal seismology (SCS) is an enterprise that unites theories and observations, as was clear in the early studies where SCS was practiced implicitly (e.g., Billings 1959; Parks & Winckler 1969; Rosenberg 1970) or advocated explicitly (e.g., Uchida 1970; Roberts et al. 1984). Modern SCS remains to rely on the wealth of measurements of low-frequency waves and oscillations in the structured solar corona (see the reviews by e.g., Nakariakov & Verwichte 2005; De Moortel & Nakariakov 2012; Nakariakov & Kolotkov 2020). Also key to SCS is the increasing refinement of magnetohydrodynamic (MHD) theories for waves in structured media (see the reviews by e.g., Roberts 2000; Goossens et al. 2011; Mathioudakis et al. 2013; Nakariakov et al. 2016; also the textbooks by Goedbloed et al. 2019; Roberts 2019). Such terms as kink and sausage modes have been in routine use since their introduction to the solar context for cylindrical (Edwin & Roberts 1983; see also Zajtsev & Stepanov 1975; Spruit 1982; Cally 1986) and slab equilibria (Edwin & Roberts 1982; see also Ionson 1978; Wentzel 1979). Observationally, kink waves and oscillations have been frequently imaged in extreme ultraviolet (EUV) in both magnetically open (see the review by Banerjee et al. 2021, and references therein) and magnetically closed structures (see Nakariakov et al. 2021 for a recent review; see also Zimovets & Nakariakov 2015; Nechaeva et al. 2019 for catalogs). However, the reported instances of coronal fast sausage waves are only sporadic and exclusively connected to quasi-periodic pulsations (QPPs) in solar flares (see e.g., Van Doorselaere et al. 2016; McLaughlin et al. 2018; Li et al. 2020; Zimovets et al. 2021, for recent reviews). In particular, they have not been reported or even implicated in oscillating active region (AR) loops to our knowledge. This study is intended to address the rarity of fast sausage waves in AR loops, emphasizing conceptual understandings rather than digging into the seismological potential.

It proves necessary to detail the pertinent nomenclature. We adopt linear, pressureless, ideal, MHD throughout, focusing on straight, field-aligned equilibria that are structured only in one transverse direction. Only axial standing sausage waves are of interest, with the axial wavenumber denoted by k . The necessary terms are worded in a way that they apply to both slab and cylindrical configurations, in which some interior (denoted by the subscript i) is density-enhanced relative to its exterior (subscript e). Consider the cylindrical geometry for now. By r and R we denote the transverse coordinate and the nominal cylinder radius, respectively. By “modes” we broadly refer to the solutions to the pertinent eigenvalue problems (EVPs) defined on the open domain $[0, \infty)$, with a mode jointly characterized by some “mode frequency” and “mode function”. A mode is not necessarily an eigenmode despite the broad term “eigenvalue problem”. We reserve the term “eigenmodes” for those that qualify as such, deeming “eigenfrequencies” and “eigenfunctions” as applicable only to eigenmodes¹. Eigenvalues are necessarily real-valued in ideal MHD (see e.g., Andries & Goossens 2007; Oliver et al. 2014, 2015 hereafter AG07; ORT14; ORT15, respectively)². Eigenfunctions can then be made real-valued, enabling an eigenmode to be classified as either evanescent or oscillatory. By “evanescent eigenmodes” we refer to those for which the eigenfunctions

¹ In our context, the distinction between modes and eigenmodes is necessary only for EVPs defined on an open domain given the subtleties with the boundary condition (BC) at infinity. The specification of BCs is straightforward if a closed domain is adopted, all solutions qualifying as eigenmodes in terms of orthogonality and completeness (e.g., Courant & Hilbert 1989).

² This does not contradict the notion of ideal quasi-modes (see Chapter 10 in Goedbloed et al. 2019; also Section 3 in Goossens et al. 2014). Take resonantly damped kink motions in a cylinder where the density varies continuously over some transition layer (TL) around the boundary. For thin TLs, Soler & Terradas (2015) showed that the coordinated kink motions can maintain their global character, making their temporal variation describable by the complex frequencies computed with either the dissipative eigenmode approach (e.g., Poedts & Kerner 1991) or the ideal quasi-mode approach (e.g., Soler et al. 2013). However, the meaning of quasi-modes becomes less and less clear when the TL width increases.

in the exterior are evanescent somewhere, whereas by “oscillatory eigenmodes” we refer to those whose eigenfunctions are oscillatory throughout the exterior. Overall, two groups of EVPs have been extensively examined in the literature, the difference being in the treatment of the nominal outer boundary ($r \rightarrow \infty$). No boundary condition (BC) is specified in one group (“EVP open noBC” hereafter), whereas the BC for the other group (“EVP open noIC”) is that no incoming waves are allowed.

Now consider the simplest case where the equilibrium density takes a step profile, evaluating to ρ_i (ρ_e) where $r < R$ ($r > R$). Let v_{Ai} and v_{Ae} denote the Alfvén speeds evaluated with ρ_i and ρ_e , respectively. A series of cutoff axial wavenumbers $\{k_{\text{cutoff},m}\}$ are relevant, satisfying $k_{\text{cutoff},1} < k_{\text{cutoff},2} < \dots$ (e.g., Roberts et al. 1984; Vasheghani Farahani et al. 2014). By relevant we mean that a discrete set of m evanescent eigenmodes is allowed when $k > k_{\text{cutoff},m}$, their real-valued frequencies being consistently lower than the critical frequency $\omega_{\text{crit}} = kv_{Ae}$. The focus of the classic study by Edwin & Roberts (1983), this set is actually the evanescent part of the solutions to both “EVP open noBC” (ORT15) and “EVP open noIC” (e.g., Cally 1986; Chen et al. 2015). Note that this evanescent set is empty when $k < k_{\text{cutoff},1}$. Note also that evanescent eigenmodes are customarily referred to as “trapped modes” (e.g., Edwin & Roberts 1983; Nakariakov & Verwichte 2005; Nakariakov & Kolotkov 2020). The key difference between “EVP open noIC” and “EVP open noBC” is then that, for arbitrary k , an infinity of discrete leaky modes (DLMs) with complex-valued frequencies arise for the former (e.g., Meerson et al. 1978; Spruit 1982; Cally 1986), whereas a continuum of oscillatory eigenmodes with real-valued frequencies arises for the latter (ORT15; see also AG07; ORT14). Now focus on the situation where $k < k_{\text{cutoff},1}$, which tends to be the only situation relevant for AR loops given their large length-to-radius ratios and mild density contrasts (Aschwanden et al. 2004). A multitude of initial value problem (IVP) studies have established that DLMs, while not eigenmodes per se, may account for a substantial fraction of the system evolution (e.g., Terradas et al. 2007; Nakariakov et al. 2012; Chen et al. 2015; Guo et al. 2016)³. On the other hand, it is well known that $P^{\text{DLM}} := 2\pi/\Re\omega^{\text{DLM}} < 2.6R/v_{Ai}$ and $\tau^{\text{DLM}}/P^{\text{DLM}} := |\Re\omega^{\text{DLM}}/\Im\omega^{\text{DLM}}|/(2\pi) \sim (\rho_i/\rho_e)/\pi^2$, with P^{DLM} and τ^{DLM} representing the period and damping time, respectively (e.g., Kopylova et al. 2007). Sausage perturbations are therefore difficult to observe in AR loops given their short periodicities and rapid attenuation.

Do sausage perturbations remain difficult to observe in AR loops for other profiles of the equilibrium density ρ_0 ? This question is sensible given the intricacies for quantifying the transverse density profiles with, say, EUV measurements (see e.g., Aschwanden et al. 2003; Pascoe et al. 2017; Goddard et al. 2017). We proceed with the choice labeled “outer μ ” in Yu et al. (2017), where ρ_0 evaluates to ρ_i when $r < R$ but otherwise reads $\rho_e + (\rho_i - \rho_e)(r/R)^{-\mu}$. Here R is some nominal cylinder radius, and $\mu \geq 1$ represents some steepness parameter. Lopin & Nagorny (2015a, hereafter LN15a) were the first to examine an EVP of the “EVP open noBC” type for this family of density profiles⁴, focusing on the behavior of the solutions at infinity to single out evanescent eigenmodes. Two distinct regimes were shown to arise as dictated by μ . A series of cutoff axial wavenumbers $\{k_{\text{cutoff},m}\}$ exist when $\mu \geq 2$, satisfying $k_{\text{cutoff},1} \leq k_{\text{cutoff},2} \leq \dots$ (see also Li et al. 2018). The behavior of evanescent eigenmodes is therefore qualitatively the same as in the step case. More interesting is

³ See, e.g., Figure 3 in Terradas et al. (2007) for the temporal evolution of a sausage perturbation with $k < k_{\text{cutoff},1}$. Figures 6 and 7 therein further suggest that the leaky phase occurs only in a brief interval for the temporal evolution of kink perturbations, which are beyond the scope of this study.

⁴ The theoretical analyses in LN15a are not specific to the “outer μ ” family, for which our discussions here follow directly from the more general results therein.

the regime where $\mu < 2$, for which LN15a showed that cutoff wavenumbers become irrelevant in that evanescent eigenmodes are permitted for arbitrary k , regardless of μ and ρ_i/ρ_e . Furthermore, the frequencies of evanescent eigenmodes tend to the critical frequency $\omega_{\text{crit}} = kv_{\text{Ae}}$ when $kR \rightarrow 0$. Note that this ω_{crit} translates into a period $2L/v_{\text{Ae}}$ for axial fundamentals with L being the loop length. LN15a (see also Lopin & Nagorny 2019) accepted the dominance of evanescent eigenmodes, arguing that sausage perturbations may be invoked to account for flare QPPs with quasi-periods of both $\mathcal{O}(R/v_{\text{Ai}})$ and $\mathcal{O}(L/v_{\text{Ae}})$. Now focus again on AR loops. One deduces that sausage perturbations may be readily captured in observations for AR loops with $\mu < 2$, given the likely dominance of evanescent eigenmodes and the long periodicities. However, this deduction was not seen in the IVP study by Li et al. (2022, Paper I). For $\mu > 2$ and $\mu < 2$ alike, the sausage perturbations are subject to rapid attenuation, and their periodicities are consistently $\mathcal{O}(R/v_{\text{Ai}})$ before the signals become too weak to be of observational relevance.

This study aims to examine sausage perturbations in a slab configuration with the “outer μ ” type of equilibrium density profiles. Our motivations are threefold. Firstly, sausage perturbations in slab configurations prove to be relevant for oscillatory signals observed in a broad range of passbands, some examples being those in EUV (e.g., Verwichte et al. 2005) and radio (e.g., Roberts et al. 1983; Karlický et al. 2011; Jelínek & Karlický 2012; Kolotkov et al. 2021). Secondly, the mathematical treatments are less involved for slab than for cylindrical configurations, making it easier to concentrate on conceptual understandings. Thirdly, the EVP study by Lopin & Nagorny (2015b, LN15b hereafter) demonstrated that the behavior of cutoff wavenumbers in slab configurations is qualitatively identical to its cylindrical counterpart⁵, thereby warranting a slab version of the IVP study by Paper I. We nonetheless stress that this study is new in the following aspects. One, we will consistently solve the IVP in terms of eigensolutions to an EVP defined on a closed domain. This “Modal Closed” approach has been employed only in the cylindrical studies on sausage perturbations by Berghmans et al. (1996) and Paper I to our knowledge. Two, we will revisit the IVP study for step density profiles by AG07, offering a Fourier-integral-based formal solution rather than following the Laplace transform approach therein. Key to this formal solution are the eigensolutions to an EVP of the “EVP open noBC” type (see ORT14; ORT15; Paper I). Our study complements AG07 by further addressing the connection between continuum eigenmodes and discrete leaky modes. We will additionally demonstrate how the oscillatory continuum for open systems is recovered by the discrete eigenspectrum in our “Modal Closed” approach. Three, we will work on the more general situation with finite μ , paying special attention to the influence of μ on the connection between the discrete eigenspectrum and the oscillatory continuum.

This manuscript is structured as follows. We formulate the IVP for a laterally open system in Section 2, where we also detail the “Modal Closed” approach. Section 3 then largely proceeds analytically to examine the IVP for a step density profile. We move on to numerically examine the more general situation where μ is finite in Section 4. Section 5 summarizes the present study, ending with some concluding remarks.

⁵ By this assertion we mean that cutoff axial wavenumbers exist only when $\mu \geq 2$, for slab and cylindrical geometries alike (see Li et al. 2018, Figure 8). The mode functions, however, differ quantitatively in their dependencies on the transverse coordinate. Consider trapped sausage modes in coronal equilibria with step density profiles. The transverse velocity in the exterior follows $K_1(\kappa_e r)$ ($e^{-\kappa_e x}$) for cylindrical (slab) equilibria, with $\kappa_e = \sqrt{k^2 - \omega^2/v_{\text{Ae}}^2}$ and K_1 the modified Bessel function of the second kind (e.g., Roberts 2019). The former profile tends to drop off more rapidly with distance. We note by passing that the same difference in the drop-off rate takes place for trapped kink modes as well (see e.g., Goossens et al. 1992; Arregui et al. 2007a; Hindman & Jain 2021; Yu et al. 2021 for the connection between the two geometries).

2. PROBLEM FORMULATION

2.1. *Equilibrium and Overall Description*

We work in the framework of pressureless, ideal, MHD throughout. Let ρ , \mathbf{v} , and \mathbf{B} denote the mass density, velocity, and magnetic field, respectively. We denote the equilibrium quantities with a subscript 0, and assume that the equilibrium is static ($\mathbf{v}_0 = 0$). Working in a Cartesian coordinate system (x, y, z) , we take the equilibrium magnetic field to be uniform and z -directed ($\mathbf{B}_0 = B_0 \mathbf{e}_z$). We assume that the equilibrium density (ρ_0) depends only on x and is symmetric about $x = 0$. Specifically, $\rho_0(x)$ is chosen to be the ‘‘outer μ ’’ family in Yu et al. (2017),

$$\begin{aligned} \rho_0(x) &= \rho_e + (\rho_i - \rho_e)f(x), \\ f(x) &= \begin{cases} 1, & 0 \leq x \leq R, \\ (x/R)^{-\mu}, & x \geq R. \end{cases} \end{aligned} \quad (1)$$

Here R represents some nominal slab half-width. With the subscript i (e) we denote the equilibrium quantities at $x = 0$ ($x \rightarrow \infty$). The Alfvén speed is defined by $v_A^2 = B_0^2/(\mu_0 \rho_0)$ with μ_0 being the magnetic permeability of free space. By v_{Ai} (v_{Ae}) we then refer to the Alfvén speed at the slab axis (infinitely far). Evidently, the steepness parameter μ is such that ρ_0 (v_A) decreases (increases) more rapidly with x towards ρ_e (v_{Ae}) when μ increases.

Let the subscript 1 denote small-amplitude perturbations. We neglect both out-of-plane propagation ($\partial/\partial y = 0$) and the out-of-plane components of vectorial quantities. Consequently, only v_{1x} , B_{1x} , and B_{1z} survive in linearized, pressureless, ideal MHD. With axial standing waves in mind, we take coronal slabs to be bounded by the planes $z = 0$ and $z = L$, and adopt the following ansatz

$$\begin{aligned} v_{1x}(x, z, t) &= \hat{v}(x, t) \sin(kz), \\ B_{1x}(x, z, t) &= \hat{B}_x(x, t) \cos(kz), \\ B_{1z}(x, z, t) &= \hat{B}_z(x, t) \sin(kz), \end{aligned} \quad (2)$$

where $k = n\pi/L$ is the quantized axial wavenumber ($n = 1, 2, \dots$). One finds that \hat{B}_x and \hat{B}_z are connected to \hat{v} via

$$\frac{\partial \hat{B}_x}{\partial t} = k B_0 \hat{v}, \quad (3)$$

$$\frac{\partial \hat{B}_z}{\partial t} = -B_0 \frac{\partial \hat{v}}{\partial x}. \quad (4)$$

We assume that

$$\hat{B}_x(x, t = 0) = \hat{B}_z(x, t = 0) = 0 \quad (5)$$

without loss of generality. The initial velocity perturbation is taken to be

$$u(x) := \hat{v}(x, t = 0) = \begin{cases} v_{Ai} \sin^3(\pi x/\Lambda), & 0 \leq x \leq \Lambda, \\ 0, & x \geq \Lambda, \end{cases} \quad (6)$$

which is localized within $x = \Lambda$ and prescribed to be sufficiently smooth with a magnitude arbitrarily set to be v_{Ai} . Only sausage perturbations arise given that $u(x = 0) = 0$ and that $\rho_0(x)$ is even. It suffices to consider only the half-plane $x \geq 0$.

2.2. Initial Value Problem and Energetics

We retain only \hat{v} to formulate our IVP for convenience.

IVP 1 *Solutions are sought for the following equation*

$$\frac{\partial^2 \hat{v}}{\partial t^2} = v_A^2(x) \left(\frac{\partial^2 \hat{v}}{\partial x^2} - k^2 \hat{v} \right), \quad (7)$$

subject to the initial conditions (ICs)

$$\hat{v}(x, t = 0) = u(x), \quad \frac{\partial \hat{v}}{\partial t}(x, t = 0) = 0, \quad (8)$$

together with the boundary condition (BC)

$$\hat{v}(x = 0, t) = 0, \quad (9)$$

on a domain spanning from $x = 0$ to ∞ .

Note that no BC is required at $x \rightarrow \infty$. Note further that the IC for $\partial \hat{v} / \partial t$ is based on the IC (5), from which $\hat{B}_x(x, t)$ and $\hat{B}_z(x, t)$ can be found by integrating Equations (3) and (4) over time once $\hat{v}(x, t)$ is known.

It proves necessary to examine the associated energetics. Let \mathcal{V} refer to a volume that is of unit length in the y -direction and spans the rectangle $[0, x] \times [0, L]$ in the $x - z$ plane. An energy conservation law is then readily derived, reading

$$E_{\text{tot}}(x, t) - E_{\text{tot}}(x, t = 0) = -F(x, t), \quad (10)$$

where

$$E_{\text{tot}}(x, t) = \frac{L}{2} \int_0^x dx' \left\{ \frac{1}{2} \rho_0(x') \hat{v}^2(x', t) + \frac{1}{2\mu_0} \left[\hat{B}_x^2(x', t) + \hat{B}_z^2(x', t) \right] \right\}, \quad (11)$$

$$F(x, t) = \frac{L}{2} \int_0^t dt' [\hat{p}_T(x, t') \hat{v}(x, t')] . \quad (12)$$

Here $\hat{p}_T = B_0 \hat{B}_z / \mu_0$ represents the Eulerian perturbation of total pressure, and the terms in the square parentheses in Equation (12) stem from the lateral component of the Poynting vector. Furthermore, the common factor $L/2$ is retained to ensure that $E_{\text{tot}}(x, t)$ represents the instantaneous total energy in \mathcal{V} , while $F(x, t)$ represents the cumulative energy loss from \mathcal{V} .

2.3. Solution Methods

We choose to solve IVP 1 with two independent methods, one being a finite-difference (FD) approach, and the other being a modal approach involving eigensolutions to an EVP on a finite domain. The modal solutions turn out to be more physically insightful. The FD approach, however, is orders-of-magnitude less time-consuming. Two situations then arise where we present the FD solutions. First, different approaches may need to be cross-validated. Second, parametric studies are needed or the FD approach is more convenient to work with.

2.3.1. The Finite-Difference Approach

Our FD scheme is second-order accurate in both space and time, and is essentially identical to its cylindrical counterpart in [Paper I](#). A uniform grid with spacing $\Delta x = 0.01 R$ is employed for simplicity. The timestep is specified as $\Delta t = c\Delta x/v_{\text{Ae}}$, where the Courant number c is chosen to be ~ 0.4 to maintain numerical stability. We ensure that no difference can be discerned when Δx or c varies. More importantly, we make sure that our FD solutions remain the same when the outer boundary is placed at larger distances.

2.3.2. The “Modal Closed” Approach

Our modal approach, labeled “Modal Closed” hereafter, relies on the following EVP.

EVP 1 *Nontrivial solutions are sought for the following equation*

$$\omega^2 \check{v} = -v_{\text{A}}^2(x) \left(\frac{d^2}{dx^2} \check{v} - k^2 \check{v} \right) \equiv \mathcal{L} \check{v}, \quad (13)$$

defined on a domain of $[0, d]$ and subject to the BCs

$$\check{v}(x=0) = \check{v}(x=d) = 0. \quad (14)$$

Equation (13) is found by replacing \hat{v} with $\Re[\check{v}(x) \exp(-i\omega t)]$ in Equation (7). One readily recognizes that the operator \mathcal{L} is Hermitian under the definition of the scalar product

$$\langle U|V \rangle^{(d)} \equiv \int_0^d U^*(x)V(x)\rho_0(x)dx, \quad (15)$$

where the asterisk represents complex conjugate. The superscript (d) is meant to emphasize that EVP 1 is defined on a closed domain. The following general properties (GPs) then follow from general theory.

GP 1 *The countable infinity of positive eigenvalues $\{\omega_l^2\}$ form a monotonically increasing sequence with respect to the mode number $l = 1, 2, \dots$.*

GP 2 *The l -th eigenvalue for a domain never exceeds the l -th eigenvalue for its subdomain.*

GP 3 *The l -th eigenfunction $\check{v}_l(x)$ can be made real-valued, possessing $l - 1$ nodes inside the domain.*

GP 4 *The set $\{\check{v}_l(x)\}$ is complete, satisfying the orthogonality condition*

$$\langle \check{v}_l | \check{v}_{l'} \rangle^{(d)} = \langle \check{v}_l | \check{v}_l \rangle^{(d)} \delta_{l,l'}, \quad (16)$$

where $\delta_{l,l'}$ denotes the Kronecker delta.

We specialize to our equilibrium density profile (1) from here onward. To start, the eigenfrequency ω_l can be expressed formally as

$$\frac{\omega_l R}{v_{\text{Ai}}} = \mathcal{F}_l(\rho_i/\rho_e, \mu; kR; d/R). \quad (17)$$

We see ω_l as positive without loss of generality. It now proves helpful to put Equation (13) in a Schrödinger form as

$$\frac{d^2\check{v}}{dx^2} + Q(x)\check{v} = 0, \quad (18)$$

where the coefficient $Q(x)$ is defined through a potential $V(x)$ as

$$V(x) = k^2 v_A^2(x), \quad Q(x) = \frac{\omega^2 - V(x)}{v_A^2(x)} = \frac{\omega^2}{v_A^2(x)} - k^2. \quad (19)$$

The following specific properties (SPs) of EVP 1 then ensue, where by “specific” we mean that the properties are more or less specific to our equilibrium density profile. Nonetheless, they hold regardless of the specific values of $[\rho_i/\rho_e, \mu, kR, d/R]$.

SP 1 *The eigenfrequency ω_l for any l is bound to exceed kv_{Ai} .*

SP 2 *High-frequency eigenmodes with $\omega_l^2 \gg \omega_{\text{crit}}^2 = (kv_{Ae})^2$ are always permitted, following*

$$\omega_l \approx l\pi(v_{Ae}/d), \quad \text{provided that } l^2 \gg (kd/\pi)^2. \quad (20)$$

SP 3 *The eigenfunction \check{v}_l is oscillatory where $\omega_l^2 > V(x)$ but evanescent otherwise.*

We note that SP 1 can be justified by the heuristic argument that if $\omega_l < kv_{Ai}$, then \check{v}_l necessarily cusps somewhere in the domain and therefore the continuity requirement for $d\check{v}_l/dx$ is violated. The same argument was first offered by Berghmans et al. (1996) in cylindrical geometry. Likewise, a similar version of SP 2 holds in cylindrical geometry as detailed in Appendix B in Paper I. Following the WKB treatment therein yields Equation (20) for the Cartesian geometry, and the range of validity turns out to be less restrictive. Important for this study is SP 3, with which we classify the eigenmodes for a finite d/R into two groups by the spatial behavior of the corresponding eigenfunctions. An eigenmode, labeled by l , is said to be evanescent if its eigenfunction is evanescent somewhere in the domain. In contrast, an eigenmode is deemed oscillatory if its eigenfunction is oscillatory throughout. Now that $v_A(x)$ increases monotonically toward v_{Ae} when x increases, an eigenmode is necessarily oscillatory for a given d/R if $\omega_l > \omega_{\text{crit}} = kv_{Ae}$ but evanescent when the opposite is true. Furthermore, if an eigenmode transitions from an oscillatory to an evanescent one when d/R exceeds some critical value, then property GP 2 dictates that it will remain an evanescent eigenmode for larger still d/R .

We now connect EVP 1 to the general EVP analysis in LN15b. Put briefly, the EVP therein belongs to the “EVP open noBC” category because the authors analyzed the behavior of mode functions at infinity rather than specifying some BC beforehand. The following deductions can be made by specializing to our profile $f(x)$ (see Equation (1)). Consider the situation $\mu \geq 2$ first. Equations (12) to (16) in LN15b mean that there exist a series of cutoff axial wavenumbers $k_{\text{cutoff},m}$ with $m = 1, 2, \dots$. Li et al. (2018) further showed that $k_{\text{cutoff},m}$ is expressible as

$$k_{\text{cutoff},m}R = \frac{g_m}{\sqrt{\rho_i/\rho_e - 1}} \quad (m = 1, 2, \dots), \quad (21)$$

where the ρ_i/ρ_e -independent coefficient $g_m \geq 1/2$. One then deduces that no evanescent eigenmodes are permitted if $k < k_{\text{cutoff},1}$, with the inequality bound to hold when

$$kR < \frac{1/2}{\sqrt{\rho_i/\rho_e - 1}}. \quad (22)$$

Now consider the situation where $\mu < 2$, for which Equations (18) and (19) in LN15b lead to the peculiar behavior for cutoff wavenumbers to disappear altogether. However, what needs to be treated with caution is not this peculiarity but the assertion that “all fast modes are trapped” for any k and hence “such plasma slab configurations behave as perfect waveguides” (page 3, LN15b) in view of our EVP 1. Our point is, an infinity of oscillatory eigenmodes are ensured by property SP 2 regardless of d/R , making them difficult to disappear altogether in the limit $d/R \rightarrow \infty$. More importantly, the solution to IVP 1 at any location can be expressed in terms of the eigensolutions to EVP 1 provided that a timeframe of validity is specified. Ideally, this confusion should be resolved with a theoretical understanding of the spectrum associated with the EVP examined in LN15b. However, we argue that there is no need to do so as long as the solutions to IVP 1 can be understood with the aid of the textbook properties of EVP 1. In particular, the “Modal Closed” approach allows to make clear what is meant by the irrelevance of cutoff wavenumbers. We therefore restrict ourselves to the situation where Inequality (22) holds.

Some remarks remain necessary on the role of μ for EVP 1 when $k < k_{\text{cutoff},1}$. To start, property GP 2 follows from Theorem 3 in Courant & Hilbert (1989, Chapter VI), where it was noted that the l -th eigenvalue for a domain is in fact smaller than the l -th eigenvalue for any of its subdomains. When $\mu \geq 2$, one then directly deduces that EVP 1 allows only oscillatory eigenmodes for any finite domain, because evanescent eigenmodes are prohibited for a truly open domain. For $\mu < 2$, on the other hand, some concern may arise when we compute evanescent eigenmodes for EVP 1. Let l refer to an evanescent eigenmode, and let $\omega_l(d)$ be its eigenfrequency evaluated with a domain of size d . The stronger version of property GP 2 then dictates that the eigenfrequency ω_l depends on the domain size, meaning specifically that $\omega_l(d') < \omega_l(d)$ for any $d' > d$. In practice, however, we need to quote some domain-independent eigenfrequency for definiteness (e.g., Figure 8). This discrepancy is nonetheless only apparent, because what we mean by domain-independent is that $\omega_l(d')$ and $\omega_l(d)$ are equal within the accuracy of our numerical solver when d is sufficiently large.

With the above preparations, the “Modal Closed” solution to IVP 1 writes

$$\hat{v}^{(d)}(x, t) = \sum_{l=1}^{\infty} c_l \check{v}_l(x) \cos(\omega_l t), \quad (23)$$

$$0 \leq x \leq d, \quad t \leq \int_{\Lambda}^d \frac{dx}{v_A(x)}.$$

Here the coefficient c_l measures the contribution from the l -th eigenmode,

$$c_l = \frac{\langle u | \check{v}_l \rangle^{(d)}}{\langle \check{v}_l | \check{v}_l \rangle^{(d)}}. \quad (24)$$

Despite the superscript (d) , we stress that $\hat{v}^{(d)}(x, t)$ itself does not depend on d as long as the outermost edge of the perturbation has not reached $x = d$. The relevant timeframe of validity is explicitly specified in Equation (23).

Two steps are involved for numerically evaluating the “Modal Closed” solution. Firstly, we follow Paper I to formulate and solve EVP 1 with the general-purpose finite-element code PDE2D (Sewell 1988), which was introduced into the solar context by Terradas et al. (2005a)⁶. As output

⁶ PDE2D has subsequently been extensively employed in solar wave studies for addressing both IVPs (e.g., Terradas et al. 2006; Soler & Goossens 2011; Oliver et al. 2016) and EVPs (e.g., Arregui et al. 2007b, 2011; Chen et al. 2021). Recently, it found application to the construction of magnetohydrostatic equilibria as well (Terradas et al. 2022).

we have the sets $\{\omega_l\}$ and $\{\check{v}_l\}$ for a specified combination $[\rho_i/\rho_e, \mu; kR; d/R]$. Secondly, we evaluate the coefficient c_l and then the modal solution $\hat{v}^{(d)}$ with Equations (24) and (23), respectively. We ensure that a sufficient number of eigenmodes are incorporated in the sum.

2.4. Parameter Specification

Let us start by recalling that the solution to IVP 1 is determined by the combination $[\rho_i/\rho_e, \mu; kR; \Lambda/R]$. We see the steepness parameter μ as the primary adjustable, and occasionally adjust the spatial extent Λ as well. The combination $[\rho_i/\rho_e, kR]$ is fixed at $[2.25, \pi/15]$ throughout. We examine only axial fundamentals, for which the adopted kR translates into a value of $L/R = 15$ for the ratio of the axial slab length to the nominal half-width. Note that this pair of $[\rho_i/\rho_e, L/R]$ is reasonable for AR loops, although they somehow lie close to the lower ends of the observed ranges deduced from EUV measurements (e.g., [Aschwanden et al. 2004](#); [Schrijver 2007](#)). Note further that this pair yields a $(kR)\sqrt{\rho_i/\rho_e - 1}$ of 0.23, and hence ensures Inequality (22). Figure 1a offers a two-dimensional (2D) representation of IVP 1 by presenting the $x - z$ distributions of the equilibrium density (the filled contours) and the initial velocity field (the arrows). The equilibrium density is further plotted against the transverse coordinate in Figure 1b, where two values are examined for the steepness parameter μ as labeled. In addition, the x -profile for the initial perturbation is also shown, with Λ chosen to be $4R$ for illustrative purposes.

3. STEP DENSITY PROFILE ($\mu = \infty$)

This section examines IVP 1 for the simplest situation where the equilibrium density takes a step profile. Our purposes are threefold. Firstly, the only published analytical study on IVP 1 for the present case was due to [AG07](#), who adopted a Laplace transform approach. Our Section 3.1 will present a new analytical solution by directly working with eigenmodes on an open domain within the simpler Fourier framework⁷. Secondly, in Section 3.2 we will employ our Fourier solution to address the connection between the oscillatory continuum modes and the much-studied discrete leaky modes, which in some sense makes more apparent the notion raised by [AG07](#) that the initial perturbation is of critical importance. Thirdly, in Section 3.3 we will address the connection between the oscillatory continuum and the discrete spectrum associated with EVP 1.

3.1. Formal Solution to the IVP in Terms of Eigenmodes on an Open Domain

This subsection works out the formal solution to IVP 1 in terms of eigenmodes on an open domain. The cylindrical version of this approach was presented in Appendix A.1 of [Paper I](#), which in turn was based on the Fourier approach detailed by [ORT14](#) and [ORT15](#). We see the axial wavenumber k as arbitrary in this subsection. While derived for a given k , the resulting expressions can find immediate applications if a continuous distribution of k is involved such as happens for wave trains impulsively excited by localized perturbations (see [ORT14](#); [ORT15](#); also [Li et al. 2023](#)).

The EVP of interest in this subsection is of the ‘‘EVP open noBC’’ type, meaning specifically that it is defined on $[0, \infty)$ and no BC is specified at infinity. A series of cutoff wavenumbers exist and are given by

$$k_{\text{cutoff},m}R = \frac{(m - 1/2)\pi}{\sqrt{\rho_i/\rho_e - 1}}, \quad (25)$$

⁷ Only real frequencies are involved in the Fourier approach. The Laplace transform approach, on the other hand, requires contour integrals in the complex frequency plane and hence the identification of the branch cuts of the Green’s function. However, we follow [AG07](#) to stress that different expressions from different approaches are necessarily equivalent because they describe the same temporal evolution.

where $m = 1, 2, \dots$. Evidently, $k_{\text{cutoff},1} < k_{\text{cutoff},2} < \dots$. Defining

$$\begin{aligned} k_i^2 &= \frac{\omega^2 - k^2 v_{\text{Ai}}^2}{v_{\text{Ai}}^2}, \\ k_e^2 &= \frac{\omega^2 - k^2 v_{\text{Ae}}^2}{v_{\text{Ae}}^2}, \\ \kappa_e^2 &= -\frac{\omega^2 - k^2 v_{\text{Ae}}^2}{v_{\text{Ae}}^2} = -k_e^2, \end{aligned} \quad (26)$$

we note that $k_i^2 > 0$ because ω always exceeds kv_{Ai} . The eigensolutions are then discriminated by the sign of k_e^2 . Proper eigenmodes ($k_e^2 < 0$) arise when k exceeds $k_{\text{cutoff},1}$, characterized by a finite set of discrete frequencies. Let j label a proper eigenmode, whose eigenfunction then writes

$$\check{v}_j(x) = \begin{cases} -\frac{v_{\text{Ai}}}{k_i R} e^{-\kappa_e R} \sin(k_i x), & 0 \leq x \leq R, \\ \frac{v_{\text{Ai}}}{\kappa_e R} \cos(k_i R) e^{-\kappa_e x}, & x > R. \end{cases} \quad (27)$$

Evidently, proper eigenmodes are necessarily evanescent. Equation (27) is written to ensure the continuity of $d\check{v}_j(x)/dx$. The continuity of $\check{v}_j(x)$, on the other hand, yields a dispersion relation (DR) that dictates the eigenfrequency ω_j ,

$$\kappa_e \tan(k_i R) + k_i = 0. \quad (28)$$

Improper eigenmodes ($k_e^2 > 0$) are relevant regardless of k . They are characterized by a continuous frequency coverage in the range (kv_{Ae}, ∞) , and hence are oscillatory. Note that the concept of dispersion relation does not apply. We then derive the improper eigenfunction $\check{v}_\omega(x)$ by solving Equation (18) under the requirements that both \check{v}_ω and $d\check{v}_\omega(x)/dx$ be continuous across $x = R$. The result writes

$$\check{v}_\omega(x) = \begin{cases} -v_{\text{Ai}} \frac{k_e}{k_i} \sin(k_i x), & 0 \leq x \leq R, \\ -v_{\text{Ai}} [A_c \cos(k_e x) + A_s \sin(k_e x)], & x > R, \end{cases} \quad (29)$$

where

$$\begin{aligned} A_c &= \frac{k_e}{k_i} \sin(k_i R) \cos(k_e R) - \cos(k_i R) \sin(k_e R), \\ A_s &= \frac{k_e}{k_i} \sin(k_i R) \sin(k_e R) + \cos(k_i R) \cos(k_e R). \end{aligned} \quad (30)$$

We scale \check{v}_ω in such a way that it remains regular when k_e approaches zero.

We solve IVP 1 by directly superposing the proper and improper eigensolutions. This ‘‘Modal Open’’ approach is possible because the eigensolutions in the discrete proper set and the improper continuum are complete, satisfying the orthogonality condition

$$\begin{aligned} \langle \check{v}_j | \check{v}_{j'} \rangle^{(\infty)} &= \langle \check{v}_j | \check{v}_j \rangle^{(\infty)} \delta_{j,j'}, \\ \langle \check{v}_j | \check{v}_\omega \rangle^{(\infty)} &= 0, \\ \langle \check{v}_\omega | \check{v}_{\omega'} \rangle^{(\infty)} &= q(\omega) \delta(\omega - \omega'). \end{aligned} \quad (31)$$

Here the scalar product is defined as

$$\langle U|V\rangle^{(\infty)} \equiv \int_0^\infty U^*(x)V(x)\rho_0(x)dx, \quad (32)$$

and the superscript ∞ emphasizes that the eigensolutions pertain to an open domain. For the proper eigenmodes, it is straightforward to obtain that

$$\langle \check{v}_j|\check{v}_j\rangle^{(\infty)} = (\rho_i v_{Ai}^2 R) \frac{e^{-2\kappa_e R}}{2} \left[\frac{1}{k_i^2 R^2} + \frac{\cos^2(k_i R)}{\kappa_e R} \left(\frac{1}{k_i^2 R^2} + \frac{\rho_e/\rho_i}{\kappa_e^2 R^2} \right) \right]. \quad (33)$$

For the improper eigenmodes, however, some algebra is necessary for evaluating $q(\omega)$ in front of the generalized function $\delta(\omega - \omega')$ in Equation (31). The net result is that

$$q(\omega) = (\rho_e v_{Ai}^2) \frac{k_e v_{Ae}^2}{\omega} \frac{\pi(A_c^2 + A_s^2)}{2}. \quad (34)$$

The ‘‘Modal Open’’ solution to IVP 1 eventually writes

$$\hat{v}(x, t) = \sum_{j=1}^J c_j \check{v}_j(x) \cos(\omega_j t) + \int_{kv_{Ae}}^\infty S_\omega \check{v}_\omega(x) \cos(\omega t) d\omega, \quad (35)$$

$$0 < x < \infty, \quad 0 < t < \infty,$$

where

$$c_j = \frac{\langle u|\check{v}_j\rangle^{(\infty)}}{\langle \check{v}_j|\check{v}_j\rangle^{(\infty)}}, \quad (36)$$

$$S_\omega = \frac{\langle u|\check{v}_\omega\rangle^{(\infty)}}{q(\omega)} = \frac{\omega \langle u|\check{v}_\omega\rangle^{(\infty)}}{(\rho_e v_{Ai}^2)(k_e v_{Ae}^2)(\pi/2)(A_c^2 + A_s^2)}.$$

We view $S_\omega \check{v}_\omega(x)$ as some local spectral density. Furthermore, J counts all proper eigenmodes j that satisfy $k > k_{\text{cutoff},j}$. Evidently, $J = 0$ if $k < k_{\text{cutoff},1}$.

Some remarks are necessary. To start, proper eigenmodes are the familiar ‘‘trapped modes’’, with Equations (25) to (28) well documented in, say, Chapter 5 of Roberts (2019). Somehow less familiar is the improper continuum (kv_{Ae}, ∞) , which arises due to the absence of a BC at infinity. However, the ‘‘Modal Open’’ approach itself is actually well established, with Equation (34) resulting essentially from the techniques developed in the cylindrical study of ORT14. We nonetheless note that the formal solution (35) has not been derived this way to our knowledge. We also note that this solution is valid at arbitrary (x, t) for arbitrary k .

3.2. Discrete Leaky Modes vs. Improper Continuum Eigenmodes

This subsection aims at offering a better distinction between discrete leaky modes (DLMs) and improper continuum eigenmodes.

We start by summarizing some necessary properties of DLMs, which are solutions to an EVP of the ‘‘EVP open noIC’’ type. We define μ_i^2 and μ_e^2 in the same way as k_i^2 and k_e^2 in Equation (26), seeing ω as possibly complex-valued and assuming $-\pi/2 < \arg \mu_i, \arg \mu_e \leq \pi/2$ (e.g., Yu et al. 2015).

Note that the time-dependence of any perturbation is written as $e^{-i\omega t}$ in its Fourier decomposition. The mode function in the exterior then writes $e^{i\mu_e x}$ to within a complex-valued factor, because the other independent solution $e^{-i\mu_e x}$ to Equation (18) is connected with incoming waves. All mode frequencies are discrete, obeying the nominal DR (e.g., Terradas et al. 2005b; Yu et al. 2015)

$$i\mu_e = \mu_i \cot(\mu_i R). \quad (37)$$

Equation (37) is well known to allow solutions with purely imaginary μ_e when $k > k_{\text{cutoff},1}$. These solutions coincide with the proper eigensolutions to ‘‘EVP open noBC’’, and are therefore not of further interest. More interesting are the DLMs, which exist regardless of k . As first shown by Terradas et al. (2005b), the complex-valued frequency of the m -th DLM may be approximated by

$$\begin{aligned} \frac{R\Re\omega_m^{\text{DLM}}}{v_{\text{Ai}}} &\approx \left(m - \frac{1}{2}\right) \pi, \quad (m = 1, 2, \dots) \\ \frac{R\Im\omega_m^{\text{DLM}}}{v_{\text{Ai}}} &\approx -\frac{1}{2} \ln \frac{1 + \sqrt{\rho_e/\rho_i}}{1 - \sqrt{\rho_e/\rho_i}}, \end{aligned} \quad (38)$$

provided that $|\omega_m^{\text{DLM}}|^2 \gg k^2 v_{\text{Ae}}^2$. That DLMs do not qualify as eigenmodes have been pointed out in the cylindrical study by ORT15. The same holds for the Cartesian version, to corroborate which we add that no scalar product can be properly defined for the relevant EVP. That said, it is known that the periods and damping times predicted with Equation (37) may describe a substantial portion of the time sequences of the relevant perturbations (e.g., Terradas et al. 2005b; Hornsey et al. 2014; Yu et al. 2015). Whether this happens is solely determined by how the initial perturbation $u(x)$ is prescribed, a notion highlighted by AG07. We will visualize this notion by several specific computations, which in a sense makes the notion more concrete.

Figure 2 presents the ‘‘Modal Open’’ solutions (Equation (35), the solid curves) to the $\mu = \infty$ version of IVP 1. Only the improper continuum needs to be considered, given that $[\rho_i/\rho_e, kR]$ is fixed at $[2.25, \pi/15]$. A number of values are examined for the spatial extent of the initial perturbation (Λ) as discriminated by the different colors. The lateral speeds at the nominal half-width $\hat{v}(R, t)$ as functions of time are plotted in Figure 2a, where the finite difference (FD) solutions are shown by the symbols for comparison. Note that the FD solutions are shown only for $\Lambda/R = 1$ and $\Lambda/R = 2$ to avoid further crowding the curves. Nonetheless, it holds in general that the FD solutions agree exactly with the ‘‘Modal Open’’ ones, thereby validating both approaches. More importantly, one sees that the temporal profile involves increasingly fine scales as Λ decreases. This behavior is then quantified in Figure 2b, where the local spectral densities $S_\omega \check{v}_\omega(R)$ are shown against the frequency ω . The critical frequency $\omega_{\text{crit}} = kv_{\text{Ae}}$ is given by the vertical dash-dotted line for reference. In agreement with Figure 2a, one sees that improper eigenmodes with increasingly high frequencies are involved when Λ decreases. Furthermore, one sees that the local spectral densities tend to favor a set of discrete frequencies indicated by the arrows, which represent the real parts of the mode frequencies ($\{\Re\omega_m^{\text{DLM}}\}$) of the first several DLMs as found by numerically solving Equation (37). Some further inspection indicates that the values for the set $\{\Re\omega_m^{\text{DLM}}\}$ can be safely approximated by Equation (38), which is not surprising given that the inequality $|\omega_m^{\text{DLM}}|^2 \gg k^2 v_{\text{Ae}}^2$ holds well. Equally unsurprising is that these frequencies tend to stand out in $S_\omega \check{v}_\omega(R)$, for they tend to do so in S_ω . We capitalize on the expression for S_ω (see Equation (36)) to explain this, and focus for now on the

situation where $\omega^2 \gg k^2 v_{\text{Ae}}^2$. It then follows that $k_i^2 \approx \omega^2/v_{\text{Ai}}^2$ and $k_e^2 \approx \omega^2/v_{\text{Ae}}^2$. Consequently, the ω -dependence of S_ω is largely determined by the factor $A_c^2 + A_s^2$, which in turn approximates to

$$A_c^2 + A_s^2 \approx \rho_e/\rho_i + (1 - \rho_e/\rho_i) \cos^2(\omega R/v_{\text{Ai}}). \quad (39)$$

Evidently, the set $\{\Re\omega_m^{\text{DLM}} \approx (m - 1/2)\pi v_{\text{Ai}}/R\}$ minimizes $A_c^2 + A_s^2$ and therefore tends to maximize $|S_\omega|$. That $S_\omega \check{v}_\omega(R)$ tends to attain a local extreme at the set $\{\Re\omega_m^{\text{DLM}}\}$ is further strengthened by the fact that $\check{v}_\omega(R)$ does so given that $\check{v}_\omega(R) \approx -v_{\text{Ai}}\sqrt{\rho_e/\rho_i} \sin(\omega R/v_{\text{Ai}})$ (see Equation (29)). One therefore deduces with Equation (36) that the deviation of the locations of local extrema from $\{\Re\omega_m^{\text{DLM}}\}$ when $\omega^2 \gg k^2 v_{\text{Ae}}^2$ is almost entirely due to the specification of the initial perturbation. This deviation is reflected in two aspects. Firstly, the positions of some extrema may be slightly different from $\{\Re\omega_m^{\text{DLM}}\}$, with the first extremum for $\Lambda/R = 1$ or $\Lambda/R = 2$ being an example. Secondly, and more severely, some extrema may not be accounted for by $\{\Re\omega_m^{\text{DLM}}\}$. This is particularly true when Λ/R is large, as exemplified by the second (third) extremum for $\Lambda/R = 4$ ($\Lambda/R = 8$). Now consider the situation where the inequality $\omega^2 \gg k^2 v_{\text{Ae}}^2$ does not hold. For large Λ , one sees some further extrema that take place at frequencies below $\Re\omega_1^{\text{DLM}}$. The first extremum for $\Lambda/R = 8$ serves as an example for this aspect, and it therefore does not make much sense to further question whether the associated damping timescale agrees with the expectation with Equation (37). Rather, with Figure 2 we conclude that the details of the initial perturbation play an important role in the temporal evolution of the system.

3.3. Connection Between the ‘‘Modal Closed’’ and ‘‘Modal Open’’ Solutions

This subsection discusses the connection between the ‘‘Modal Closed’’ and ‘‘Modal Open’’ solutions, the aim being to further visualize the fact that improper continuum modes qualify as eigenmodes. For simplicity, we focus on the situation where $k < k_{\text{cutoff},1}$ such that proper modes are irrelevant.

Let us start with some analytical progress for the eigensolutions to EVP 1, which we recall is defined on a closed domain $[0, d]$. The eigenfunctions remain expressible by Equation (29), except that the eigenfrequencies are discrete as determined by the DR

$$A_c \cos(k_e d) + A_s \sin(k_e d) = 0. \quad (40)$$

Evidently, this DR is nothing but the BC at the outer boundary. Consider now low-frequency eigenmodes, by which we mean $\omega = kv_{\text{Ae}}(1 + \Delta)$ where $0 < \Delta \ll 1$. One readily recognizes from Equation (26) that $k_i^2 \approx k^2(\rho_i/\rho_e - 1)$ and $k_e^2 \approx k^2(2\Delta)$. Now suppose $k_e R \ll 1$. Equation (30) then indicates that $A_c/A_s \sim \mathcal{O}(k_e R)$, meaning that the leading order solution to Equation (40) is $k_e d \approx l\pi$. Hence $\Delta \approx (l\pi)^2/(2k^2 d^2)$. To sum up, the low-frequency eigenmodes are characterized by

$$\frac{\omega_l}{kv_{\text{Ae}}} \approx 1 + \frac{(l\pi)^2}{2(kd)^2}, \quad \text{provided that } (kd)^2 \gg (l\pi)^2, \quad d/R \gg l\pi. \quad (41)$$

Now consider high-frequency eigenmodes, by which we mean $\omega^2 \gg k^2 v_{\text{Ae}}^2$. Equation (26) indicates that $k_i \approx k_e \approx \omega/v_{\text{Ai}}$. Some algebra then leads the DR (40) to become

$$\sin[k_e(d - R) + \phi_e] \approx 0, \quad (42)$$

where ϕ_e is governed by

$$\tan \phi_e = \sqrt{\rho_e/\rho_i} \tan(\sqrt{\rho_i/\rho_e} k_e R). \quad (43)$$

One readily sees that the leading order solution is given by Equation (20), which is not surprising because this approximate expression applies to arbitrary μ . Nonetheless, the explicit DR (40) can be employed to yield the next order correction, the net result being

$$\begin{aligned}\omega_l &\approx (l\pi - \phi_l) \frac{v_{\text{Ae}}}{d - R}, \\ \phi_l &\approx \arctan \left[\sqrt{\rho_e/\rho_i} \tan \left(\sqrt{\rho_i/\rho_e} \frac{l\pi}{d/R - 1} \right) \right] + \left\lfloor \sqrt{\rho_i/\rho_e} \frac{l}{d/R - 1} + \frac{1}{2} \right\rfloor \pi,\end{aligned}\tag{44}$$

with $\lfloor \cdot \rfloor$ being the floor function. Equation (44) is presented only for completeness, the derivation for which is the same as in Appendix A.2 of Paper I.

More important to this study is that the discrete set of eigenfrequencies ω_l for EVP 1 converges to the improper continuum when the domain size d extends to infinity. Let

$$\Delta\omega_l = \omega_{l+1} - \omega_l, \quad l = 1, 2, \dots\tag{45}$$

define the frequency spacing. The continuum is then approached in such a way that $\Delta\omega_l$ starts with a $1/d^2$ dependence for small l (see Equation (41)) and transitions to a $1/d$ dependence for large l (see Equation (20)). In view of Equation (23), we define

$$S_l = \frac{c_l}{\omega_{l+1} - \omega_l}\tag{46}$$

such that $S_l \check{v}_l(x)$ represents some discrete local spectral density. Let us demonstrate that the discrete set $\{S_l \check{v}_l(x)\}$ approaches the continuous $S_\omega \check{v}_\omega(x)$ in Equation (35).

Figure 3 is similar in format to Figure 2, the primary difference being that the combination $[\rho_i/\rho_e, kR, \Lambda/R]$ is now fixed at $[2.25, \pi/15, 4]$. The “Modal Open” solution is shown by the black curves. Two domain sizes are employed for constructing the “Modal Closed” solutions, one being $d/R = 50$ (the curve and symbols in red), and the other being $d/R = 100$ (blue). Examine Figure 3a first, from which one sees that the “Modal Open” and “Modal Closed” solutions cannot be told apart. We therefore conclude with Figure 3a and Figure 2a that the “FD”, “Modal Closed”, and “Modal Open” approaches yield identical solutions to IVP 1. Now move on to Figure 3b, where the symbols represent the values of $\{S_l \check{v}_l(R)\}$ as functions of the discrete eigenfrequencies $\{\omega_l\}$ associated with the “Modal Closed” solutions. One sees that the set $\{\omega_l\}$ for $d/R = 100$ is finer than for $d/R = 50$, a feature that holds in view of Equations (41) and (20). More importantly, one sees that the sets $\{S_l \check{v}_l(R)\}$ for both values of d/R cannot be distinguished from the continuous $S_\omega \check{v}_\omega(R)$ associated with the improper continuum. We therefore conclude that the continuous $S_\omega \check{v}_\omega(R)$ can be adequately resolved with the discrete eigenmodes for a domain size as modest as $d/R = 50$. This also visualizes the general behavior for $\{S_l \check{v}_l(x)\}$ to converge to $S_\omega \check{v}_\omega(x)$ at arbitrary x .

3.4. Observational Implications

Some observational implications follow from our discussions on the connection between DLMs and the improper continuum. For clarity, we restrict our discussions to those observed signals that attenuate temporally. Our Figure 2a suggests that the quasi-periods are consistently on the order of the transverse Alfvén time R/v_{Ai} , provided that the spatial extent of the initial perturbation differs not too much from the width of the wave host. This supports the customary practice that candidate

sausage perturbations are identified primarily by their short quasi-periods (e.g., Nakariakov et al. 2003; Kolotkov et al. 2015; Carley et al. 2019). Furthermore, the formal solution (Equation (35)) stresses that the temporal damping derives from the destructive interference of the monochromatic components in the improper continuum. It then follows that a rich variety of damping envelopes may result, with the details of the initial perturbation being critical (see the expression for S_ω in Equation (36)). This damping envelope may be similar to an exponential one during some appropriate interval, and hence agree with the expectations with DLMs (e.g., Figure 4 in Terradas et al. 2005b). Conversely, nominal DRs of DLMs can be put to seismological use when some exponential damping shows up, an example being the analysis by Kopylova et al. (2007) of the flare pulsation originally reported by McLean & Sheridan (1973). However, it is equally possible, if not more common, that the damping envelope follows different patterns, given the diversity of the initial perturbations (see Figure 2a). Two consequences then arise. Firstly, there is no need to reject short-period signals as candidate sausage perturbations simply because their damping envelopes deviate from an exponential one. It is just that the meaning of the deduced damping time needs to be clarified. In this sense, one may need to re-assess the seismology performed by, say, Chen et al. (2015) for the pulsating flare emission presented in Kolotkov et al. (2015). Our point is, the seismology therein associated the damping signal with a DLM. The observed temporal damping, however, does not show a particular pattern (Kolotkov et al. 2015, Figure 3). Secondly, the details of an observed time-varying signal actually encapsulate the information on not only the wave host but also the initial perturbation. It is therefore possible, at least in principle, to decipher some appropriate flare QPPs to deduce some parameters that characterize the energy-release process. The same thinking applies to AR loops as well, if a candidate sausage perturbation is eventually identified.

4. CONTINUOUS DENSITY PROFILES ($\mu < \infty$)

This section examines the situation where μ is finite. We largely rely on the “Modal Closed” approach, and present the FD solutions only when necessary.

4.1. Comparison Between the Cases with $\mu < 2$ and $\mu > 2$

Figure 4 presents the FD solutions to IVP 1 for a fixed combination $[\rho_i/\rho_e, kR, \Lambda/R] = [2.25, \pi/15, 4]$. Two steepness parameters, $\mu = 1.5$ and $\mu = 5$, are examined as discriminated by the different colors. Note that FD solutions are shown here to avoid discussing the outer boundary, which is inherent to the “Modal Closed” approach. Figure 4 offers some gross properties of the solutions, where by gross we choose to examine the energetics in the volume \mathcal{V} within which the initial perturbation is implemented. Specifically, the total energy E_{tot} in \mathcal{V} and the cumulative energy loss F from \mathcal{V} are evaluated with Equations (11) and (12) by letting $x = \Lambda$ therein. One sees no qualitative difference between the solutions for different values of μ , despite that these values lie astride the nominally critical value of two. In both cases, E_{tot} features some rather rapid decrease with time, accompanied by some steady increase in F . The sum of the two quantities ($E_{\text{tot}} + F$) remains constant throughout, indicating that energy is conserved remarkably well (see Equation (10)). In this regard, the plateaus in E_{tot} or F arise simply because the transverse component of the Poynting vector is small during the corresponding intervals (see Equation (12)). More importantly, E_{tot} drops to extremely small values when, say, $t \gtrsim 10R/v_{\text{Ai}}$ for both μ . One then expects that the signals in the entire interval $x \leq \Lambda$ behave in a similar manner. This is indeed true, as evidenced by Figure 4b where we arbitrarily single out the transverse speed at the nominal slab half-width

$\hat{v}(R, t)$. One then sees again the rapid attenuation for both steepness parameters, with only two (four) extrema discernible when $\mu = 1.5$ ($\mu = 5$). We remark that the symbols represent the “Modal Closed” solutions constructed with Equation (23) with the domain size chosen to be $d/R = 50$. That the FD and “Modal Closed” solutions agree exactly means that this modest domain size is adequate for describing the behavior of $\hat{v}(R, t)$ in the examined timeframe.

Figure 5 capitalizes on Equation (23) to examine the contributions from individual eigenmodes. For this purpose, the discrete sets of position-independent coefficients $\{c_l\}$ and the specific contributions at the half-width $\{c_l \check{v}_l(R)\}$ are grabbed from the “Modal Closed” solutions from Figure 4. They are then plotted against the sets of eigenfrequencies $\{\omega_l\}$ in Figures 5a and 5b, with the two different steepness parameters again discriminated by the different colors. The critical frequency $\omega_{\text{crit}} = kv_{\text{Ae}}$ is given by the vertical dash-dotted lines for comparison. Examine Figure 5a first. One sees that the frequency-dependency of $|c_l|$ for $\mu = 1.5$ is qualitatively the same as that for $\mu = 5$, both featuring a series of peaks at frequencies substantially higher than ω_{crit} . Now examining Figure 5b, one sees the same set of peak frequencies in $\{c_l \check{v}_l(R)\}$ for each examined μ . The values of these peak frequencies then explain why the transverse Alfvén time R/v_{Ai} characterizes the periodicities in the signals themselves ($\hat{v}(R, t)$) shown in Figure 4b. It is just that the term “periodicity” applies only marginally to $\hat{v}(R, t)$ for $\mu = 1.5$ to say the best, given the extremely rapid attenuation of the signal. Regardless, more important is that all eigenfrequencies are above ω_{crit} , meaning that all eigenmodes are oscillatory. This is true not just for $\mu = 5$ but for $\mu = 1.5$ at least at the chosen domain size for EVP 1, despite that evanescent eigenmodes are ensured for an infinite domain when $\mu < 2$.

4.2. Dependence of Modal Structure on Domain Size

This subsection examines how the modal structure depends on the domain size d for EVP 1, where by “modal structure” we refer to the l -dependence of the eigenfrequency ω_l . Our purposes are twofold. Firstly, we will explore how the solutions to EVP 1 connect to the theoretical results on cutoff wavenumbers for an open system by LN15b. In particular, we will visualize what is meant by the irrelevance of cutoff wavenumbers when $\mu < 2$, paying special attention to how the number of evanescent eigenmodes varies with d to evaluate the assertion that “all fast modes are trapped”. Secondly, in physical terms we will demonstrate when evanescent eigenmodes are guaranteed to be negligible as far as the time-dependent solutions to IVP 1 are concerned.

Defining some fractional difference $\delta_l = \omega_l/\omega_{\text{crit}} - 1$, Figure 6 examines how its modulus varies in response to the variation of the dimensionless domain size d/R . The combination $[\rho_i/\rho_e, kR]$ is fixed at $[2.25, \pi/15]$, whereas two different values are examined for the steepness parameter, one being $\mu = 1.5$ (Figure 6a) and the other being $\mu = 5$ (Figure 6b). For each μ , we choose to always present the first five eigenmodes but sample other eigenmodes with a uniform step of five in l when the mode number l ranges from 10 to 50. The values for δ_l for any given l are connected by a solid (dashed) curve when δ_l is positive (negative). The dash-dotted curves, on the other hand, represent a $1/d^2$ dependence as inspired by the analytical result for step density profiles (see Equation (41)). Let us start with the case $\mu = 5$ as presented in Figure 6b, where one sees the unsurprising result that δ_l is consistently positive. All eigenmodes are therefore oscillatory, a behavior that can be better visualized by the spatial profiles of the first three eigenfunctions shown in the right column of Figure 7. It is also unsurprising to see that δ_l decreases monotonically with the domain size. What Figure 6b demonstrates for sufficiently large d/R is that the frequency spacing $\Delta\omega_l$ starts with a $1/d^2$ dependence for small l and gradually transitions to a $1/d$ dependence for large l , with the latter

dependence following from Equation (20). This behavior is qualitatively the same as happens for the step density profiles (see Section 3.3). We therefore conclude that a genuine continuum $(\omega_{\text{crit}}, \infty)$ can be properly defined for an open system, provided that the limit $d/R \rightarrow \infty$ is taken. However, the modal behavior for $\mu = 1.5$ is qualitatively different. One sees from Figure 6a that evanescent eigenmodes indeed show up eventually for large enough d/R , as indicated by the changes of sign of δ_l . For instance, the first eigenmode transitions from an oscillatory to an evanescent one at $d/R \approx 900$, and so does the second (third) eigenmode at $d/R \approx 6600$ ($d/R \approx 29000$). Once again, this behavior is made clearer by the spatial dependencies of the first several eigenfunctions (see the left column of Figure 7). One then deduces that an increasing number of evanescent eigenmodes emerge from the sea of oscillatory eigenmodes as the domain size increases, which we take as a visualization of the notion that cutoff wavenumbers are indeed irrelevant when $\mu < 2$. However, this notion needs to be understood as meaning that evanescent eigenmodes are always permitted for sufficiently large domains, regardless of the combination $[\rho_i/\rho_e, kR]$. On the other hand, with the exception of the lowest subset, the frequencies of oscillatory eigenmodes are such that the frequency spacing $\Delta\omega_l$ also follows a $1/d^2$ dependence at small l and gradually gives way to a $1/d$ dependence at large l . Despite this d -dependence, we conclude that a genuine continuum $(\omega_{\text{crit}}, \infty)$ cannot be defined, at least not by the straightforward limiting procedure $d/R \rightarrow \infty$ because the critical frequency is continuously crossed when d/R increases continuously. We also argue that it does not much sense to explore the spectrum for a truly open system per se, because all necessary physics can be addressed by the ‘‘Modal Closed’’ approach, which is simple both technically and conceptually. In particular, one safely concludes that evanescent eigenmodes makes no contribution to the solution to IVP 1 in Figure 4 as far as the timeframe therein is of interest, despite that a large number of evanescent eigenmodes are permitted for extraordinarily large domains. This conclusion holds because the solution in the pertinent timeframe is entirely contributed by oscillatory eigenmodes by any practical standard, and evanescent eigenmodes are incomplete no matter how dense the set of their frequencies may be.

We further exploit the ‘‘Modal Closed’’ approach to examine the condition for evanescent eigenmodes to be negligible in terms of their contributions to the system evolution. This discussion turns out to be not that straightforward. We therefore decide to employ a fixed combination $[\rho_i/\rho_e, kR] = [2.25, \pi/15]$ and additionally assume $\Lambda \geq R$. Only the situation $\mu < 2$ is relevant now. Consider some extremely large domain size d such that a substantial number of evanescent eigenmodes solve EVP 1. Let the l -th evanescent eigenmode be characterized by some spatial scale D_l , which can be unambiguously identified as the position beyond which the l -th eigenfunction is evanescent. It follows from Equation (19) that

$$\frac{D_l}{R} = \left[\frac{(1 - \alpha_l)(\rho_i/\rho_e - 1)}{\alpha_l} \right]^{1/\mu}, \quad (47)$$

where $\alpha_l = 1 - \omega_l^2/\omega_{\text{crit}}^2$. Evidently, $D_1 < D_2 < \dots$ for a given μ because $\omega_1 < \omega_2 < \dots$. For definiteness, we evaluate ω_1 at some d beyond which ω_1 does not vary with the domain size within the accuracy of our EVP solver (see Figure 6a). Figure 8a then displays $1 - \omega_1/\omega_{\text{crit}}$ and D_1 against μ . One sees that $1 - \omega_1/\omega_{\text{crit}}$ decreases and consequently D_1 increases extremely rapidly with μ , the reason being that ω_1 becomes increasingly close to ω_{crit} from below when μ approaches two.

Our following discussions center around D_1 . Immediately ensuing is a timescale τ_{D1} , namely the time at which the location $x = D_1$ is disturbed. Evidently,

$$\tau_{D1} = \int_{\Lambda}^{D_1} \frac{dx}{v_A(x)}. \quad (48)$$

Evanescent eigenmodes are guaranteed to play no role in the timeframe $t < \tau_{D1}$. Figure 8b offers an example where we survey the time-dependent solutions for a considerable number of combinations of μ and Λ . Note that the FD approach is adopted for convenience. For each $[\mu, \Lambda]$, we determine a further timescale τ_{ener} as the time at which $E_{\text{tot}}(\Lambda, t)/E_{\text{tot}}(\Lambda, t=0)$ decreases to some threshold δ_{ener} with $E_{\text{tot}}(\Lambda, t)$ being the instantaneous total energy in the volume where the initial perturbation is applied (see Figure 4). The solid curves represent the μ -dependencies of τ_{ener} determined with $\delta_{\text{ener}} = e^{-4} \approx 1/55$ for a number of Λ as discriminated by the different colors. One sees that τ_{ener} thus determined for a given Λ is largely insensitive to μ , the only exception being for $\Lambda/R = 8$ in the portion $\mu \lesssim 1.1$. There is actually some subtlety associated with this exception, as will be discussed shortly. It suffices for now to notice the overall behavior that τ_{ener} increases with Λ at a given μ . This behavior is understandable given that, when Λ increases, the eigenmodes with increasingly low frequencies make more contributions to the system evolution, thereby increasing the duration it takes for the eigenmodes to interfere to weaken $E_{\text{tot}}(\Lambda, t)$ to some threshold. Regardless, one sees that τ_{ener} at any examined $[\mu, \Lambda]$ is lower than the corresponding τ_{D1} , which is represented by the dash-dotted curves and color-coded by Λ in the same way as for τ_{ener} . This is not surprising because $\tau_{\text{ener}} \lesssim 20.8R/v_{\text{Ai}}$ with the maximum reached at $[\mu, \Lambda/R] = [1, 8]$, while Equation (48) indicates that $\tau_{D1} > (D_1 - \Lambda)/v_{\text{Ae}}$ and the latter attains a minimum of $\sim 44.2 R/v_{\text{Ai}}$ at the same $[\mu, \Lambda/R]$. The comparison between τ_{ener} and τ_{D1} therefore validates the negligible role of evanescent eigenmodes, which was explicitly shown by the specific ‘‘Modal Closed’’ solution for $[\mu, \Lambda/R] = [1.5, 4]$ (see Figures 4 and 5).

We now come back to the behavior of τ_{ener} for $\Lambda/R = 8$ as shown in Figure 8b. By subtlety we refer to the apparent discontinuity at $\mu \approx 1.1$, and refer further to the behavior of signals for $x \leq \Lambda$ in the interval $t < \tau_{D1}$. We restrict ourselves to the parametric survey presented in Figure 8 for the ease of description. The signals turn out to always evolve in three stages, to be labeled I to III hereafter. Stage I is characterized by some rapid attenuation, and the periodicity tends to be substantially shorter than $P_{\text{longi}} = 2\pi/\omega_{\text{crit}}$. Here the subscript ‘‘longi’’ is meant to indicate that this periodicity evaluates to the longitudinal Alfvén time $2L/v_{\text{Ae}}$ for axial fundamentals. In addition, $E_{\text{tot}}(\Lambda, t)$ hardly shows any increase with time. Stage III, on the other hand, is characterized by a nearly monochromatic variation with the periodicity being very close to P_{longi} . The signals still weaken with time but in a fashion different from Stage I, meaning in particular that $E_{\text{tot}}(\Lambda, t)$ is wavy and its envelope declines at a much lower rate. Stage II corresponds to the transition from Stage I to Stage III, and tends to be short in duration. The appearance of the three stages is actually a natural result of Equation (23). Stage I tends to involve eigenmodes with frequencies ω_l substantially higher than ω_{crit} , and the signals therefore tend to attenuate rapidly because the involved monochromatic components can readily interfere to largely cancel out their contributions. Consequently, modes with frequencies very close to ω_{crit} are allowed to stand out in stage III, and the associated monochromatic components require longer time to interfere to yield some appreciable attenuation. Note that the physics discussed herein only requires the negligible role of evanescent eigenmodes, and hence applies to the case for $\mu > 2$ when $k < k_{\text{cutoff},1}$. It is just that evanescent eigenmodes and τ_{D1} become

irrelevant altogether in that case, and there is no need to consider any complication beyond $t = \tau_{D_1}$. Now focus once again on Figure 8b. The details of Stage II, in particular where it is positioned in time, turn out to possess a rather intricate dependence on μ and Λ/R . One end result is that τ_{ener} always appears in Stage I for all examined pairs $[\mu, \Lambda/R]$ with the exception being for $\mu \lesssim 1.1$ when $\Lambda/R = 8$. In this case τ_{ener} appears in Stage II, and the somehow wavy behavior in $E_{\text{tot}}(\Lambda, t)/E_{\text{tot}}(\Lambda, t = 0)$ means that the threshold δ_{ener} is reached on the opposite side of a ripple to what happens for larger μ . Hence the discontinuity in the μ -dependence of τ_{ener} .

4.3. Further Remarks

The results in this section can be further digested as follows. We consistently see the interval $t \leq \tau_{\text{ener}}$ as the duration of interest, and restrict ourselves to Figures 4 and 8. Let us start with the FD solutions in Figure 4 and recall that no outer boundary is involved in IVP 1. The drop of $E_{\text{tot}}(t)/E_{\text{tot}}(t = 0)$ to the designated threshold δ_{ener} can then be explained by that almost all of the wave energy in the volume $x \leq \Lambda$ is carried away by the first two outgoing wave fronts. The passage of either front through $x = \Lambda$ is readily identified by a rapid drop in $E_{\text{tot}}(t)$ in front of a plateau-like feature. This behavior happens for both $\mu = 1.5$ and $\mu = 5$, and holds also for the cylindrical computations (see Figure 2 in Paper I). Now consider the ‘‘Modal Closed’’ solutions, and let D_{ener} denote the distance that the outermost perturbation reaches when $t = \tau_{\text{ener}}$. Furthermore, let D_{ener} be chosen as the domain size for EVP 1. By construction, the FD solution for $t \leq \tau_{\text{ener}}$ is identical to the ‘‘Modal Closed’’ solution (23) constructed with eigensolutions to EVP 1. Consequently, the outgoing fronts in the FD solution for $\mu = 5$ are in fact a manifestation of oscillatory eigensolutions, which are the only solutions to EVP 1 regardless of the domain size. Let us move on to $\mu = 1.5$, for which Figure 8b shows that $\tau_{D_1} \gg \tau_{\text{ener}}$. Hence $D_1 \gg D_{\text{ener}}$. The outgoing fronts in the FD solution for $\mu = 1.5$ then also derive from the oscillatory eigensolutions to EVP 1, given that only eigensolutions of this type are allowed for any $d < D_1$. All in all, only oscillatory eigensolutions are allowed for both $\mu = 1.5$ and $\mu = 5$ if $d = D_{\text{ener}}$. This then explains the qualitative similarity in the behavior of E_{tot} in the two FD solutions when $t < \tau_{\text{ener}}$.

Some additional implications follow. Our key message is that IVP studies in general offer a fuller picture for the wave dynamics than EVP analyses. Take the case $\mu = 1.5$ for instance. Let $d' \gg D_1$ denote another domain size for EVP 1. A considerable number of evanescent eigensolutions may be allowed together with an extremely closely spaced set of oscillatory ones. When $t < \tau_{\text{ener}}$, however, the superposition of all eigensolutions necessarily yields the same temporal behavior as computed with eigensolutions to EVP 1 on the domain of size $d = D_{\text{ener}}$. In other words, evanescent eigenmodes can be safely discarded for both the gross energetics and the signals sampled at individual locations (see Figure 4). This then calls into question the seismological applications of the EVP analyses for $\mu < 2$ by, say, Lopin & Nagorny (2015a). Of interest therein was a pulsating flare event observed by the Nobeyama Radioheliograph (NoRH) and originally reported in Kupriyanova et al. (2013). Three periodicities were found, and the spatial distributions of individual power spectral densities favor their identification as the first three axial harmonics. The interpretation of these signals as sausage perturbations was rejected by Kupriyanova et al. (2013), for the measured periods are difficult to reconcile with sausage modes in flare loops with step transverse profiles. However, Lopin & Nagorny (2015a) argued that this difficulty may be circumvented if one invokes transverse profiles similar to our ‘‘outer μ ’’ formulation with $\mu < 2$. We remark that evanescent eigensolutions were implied to dominate the system behavior for this argument to apply. Our results in this section indicate

otherwise, stressing that the physical relevance of a mode needs to be established by IVP studies before it is invoked for seismology.

5. SUMMARY

This study was motivated by some recent theoretical progresses that may cast doubt on the well-known lack of candidate sausage perturbations in solar active region (AR) loops. We adopted linear, pressureless, ideal MHD to examine the responses of straight, field-aligned, axially uniform, coronal slabs to localized initial velocity perturbations that excite axial fundamentals. The equilibrium density (ρ_0) was taken to be structured only in one lateral direction (x), following an “outer μ ” prescription where a steepness parameter μ pertains to the exterior (see Equation (1)). An initial value problem (IVP, see IVP 1) was formulated on the open domain $[0, \infty)$, to which two types of eigenvalue problems (EVPs) are relevant. No boundary condition (BC) is specified at infinity in the “EVP open noBC” type, whereas the BC at infinity for the “EVP open noIC” type is that no incoming waves are permitted. While working on an EVP of the “EVP open noBC” type, Lopin & Nagorny (2015b, LN15b) showed that the steepness of ρ_0 in the exterior is critical to the existence of cutoff axial wavenumbers. An application of the LN15b analysis to our “outer μ ” profile yields that cutoff wavenumbers arise only when $\mu \geq 2$. The lowest cutoff exceeds axial wavenumbers expected for typical AR loops (Li et al. 2018). Evanescent eigenmodes (or equivalently trapped modes) are therefore prohibited, supporting the customary argument for sausage perturbations to be difficult to detect. When $\mu < 2$, however, cutoff wavenumbers are irrelevant in that evanescent eigenmodes are always allowed regardless of the axial wavenumber (k) or the density contrast (ρ_i/ρ_e). This led LN15b to further argue that all fast waves are evanescent. By implication, sausage perturbations may then have been overlooked in AR loops with $\mu < 2$. We focused on a value of k that ensures the absence of evanescent eigenmodes for $\mu \geq 2$, and solved IVP 1 by superposing the eigenmodes on a closed domain (EVP 1; also Equation (23)). Our study can be summarized as follows.

While revisiting IVP 1 for step density profiles ($\mu \rightarrow \infty$), we offered an essentially analytical solution in terms of eigensolutions to the EVP of the “EVP open noBC” type. The importance of initial perturbations was demonstrated. In particular, their specification impacts whether the system evolution can be understood with discrete leaky modes, which arise for “EVP open noIC”. Our “Modal Closed” solutions then complemented previous studies of Andries & Goossens (2007) and Oliver et al. (2015) by visualizing how the oscillatory continuum in “EVP open noBC” is approached by the discrete eigenspectrum. We further applied the “Modal Closed” approach to the case where μ is finite, and showed that the situation with $\mu \geq 2$ is qualitatively the same as in the step case. Evanescent eigenmodes are prohibited by the relevance of cutoff axial wavenumbers, and an oscillatory continuum can result for open systems. When $\mu < 2$, we showed that cutoff wavenumbers are indeed irrelevant. However, we stressed that this irrelevance does not mean that all fast waves are evanescent for truly open systems. Rather, this means that an increasing number of evanescent eigenmodes result when the domain size increases for EVP 1. Oscillatory eigenmodes are always permitted, although a genuine continuum cannot be obtained simply by letting the domain size approach infinity. We quantified the condition for oscillatory eigenmodes to dominate the solutions to IVP 1, justifying the absence of any qualitative change of the system behavior when μ crosses the nominal critical value of two.

Before closing, we emphasize again the importance of the IVP approach for examining the wave dynamics. The physical relevance of a mode found in some EVP analysis needs to be established with

an IVP examination before it is employed for seismology. Likewise, the detailed temporal behavior of an observed oscillatory signal actually carries some rich information on both the wave host and the initial perturbation. Furthermore, we remark that our numerical findings can be summarized in a simpler way, provided that one is interested in the solutions to IVP 1 rather than any conceptual difficulty associated with the domain being open for some relevant EVPs. First of all, the mathematical properties of EVP 1 ensure that the associated eigenmodes can be used to solve IVP 1. That EVP 1 is defined on a closed domain merely means that the “Modal Closed” solution (Equation (23)) holds only in some appropriate timeframe. For our chosen parameters, the key difference in the modal behavior between $\mu \geq 2$ and $\mu < 2$ is that only oscillatory eigenmodes are allowed in the former, whereas evanescent eigenmodes eventually show up for sufficiently large domains in the latter. The system evolution, however, necessarily shows no qualitative difference for different μ in those timeframes for which the required domain sizes of EVP 1 are not large enough to accommodate evanescent eigenmodes. Only oscillatory eigenmodes are therefore involved in Equation (23). The signal at a given location then weakens with time, for the monochromatic components will interfere to cancel out their contributions. On this last aspect, we note that a close analogy can be drawn for kink waves resonantly absorbed in the Alfvén continuum (Soler & Terradas 2015; see also Cally 1991 and Andries & Goossens 2007).

We thank the referee for thorough and constructive comments. This research was supported by the National Natural Science Foundation of China (41974200, 41904150, and 11761141002). We gratefully acknowledge ISSI-BJ for supporting the international team “Magnetohydrodynamic wavetrains as a tool for probing the solar corona”.

REFERENCES

- Andries, J., & Goossens, M. 2007, *Physics of Plasmas*, 14, 052101, doi: [10.1063/1.2714513](https://doi.org/10.1063/1.2714513)
- Arregui, I., Soler, R., Ballester, J. L., & Wright, A. N. 2011, *A&A*, 533, A60, doi: [10.1051/0004-6361/201117477](https://doi.org/10.1051/0004-6361/201117477)
- Arregui, I., Terradas, J., Oliver, R., & Ballester, J. L. 2007a, *SoPh*, 246, 213, doi: [10.1007/s11207-007-9041-3](https://doi.org/10.1007/s11207-007-9041-3)
- . 2007b, *A&A*, 466, 1145, doi: [10.1051/0004-6361:20066792](https://doi.org/10.1051/0004-6361:20066792)
- Aschwanden, M. J., Nakariakov, V. M., & Melnikov, V. F. 2004, *ApJ*, 600, 458, doi: [10.1086/379789](https://doi.org/10.1086/379789)
- Aschwanden, M. J., Nightingale, R. W., Andries, J., Goossens, M., & Van Doorselaere, T. 2003, *ApJ*, 598, 1375, doi: [10.1086/379104](https://doi.org/10.1086/379104)
- Banerjee, D., Krishna Prasad, S., Pant, V., et al. 2021, *SSRv*, 217, 76, doi: [10.1007/s11214-021-00849-0](https://doi.org/10.1007/s11214-021-00849-0)
- Berghmans, D., de Bruyne, P., & Goossens, M. 1996, *ApJ*, 472, 398, doi: [10.1086/178072](https://doi.org/10.1086/178072)
- Billings, D. E. 1959, *ApJ*, 130, 215, doi: [10.1086/146710](https://doi.org/10.1086/146710)
- Cally, P. S. 1986, *SoPh*, 103, 277, doi: [10.1007/BF00147830](https://doi.org/10.1007/BF00147830)
- . 1991, *Journal of Plasma Physics*, 45, 453, doi: [10.1017/S002237780001583X](https://doi.org/10.1017/S002237780001583X)
- Carley, E. P., Hayes, L. A., Murray, S. A., et al. 2019, *Nature Communications*, 10, 2276, doi: [10.1038/s41467-019-10204-1](https://doi.org/10.1038/s41467-019-10204-1)
- Chen, S.-X., Li, B., Van Doorselaere, T., et al. 2021, *ApJ*, 908, 230, doi: [10.3847/1538-4357/abd7f3](https://doi.org/10.3847/1538-4357/abd7f3)
- Chen, S.-X., Li, B., Xiong, M., Yu, H., & Guo, M.-Z. 2015, *ApJ*, 812, 22, doi: [10.1088/0004-637X/812/1/22](https://doi.org/10.1088/0004-637X/812/1/22)
- Courant, R., & Hilbert, D. 1989, *Methods of Mathematical Physics, Vol. 1* (New York: Wiley)

- De Moortel, I., & Nakariakov, V. M. 2012, *Philosophical Transactions of the Royal Society of London Series A*, 370, 3193, doi: [10.1098/rsta.2011.0640](https://doi.org/10.1098/rsta.2011.0640)
- Edwin, P. M., & Roberts, B. 1982, *SoPh*, 76, 239, doi: [10.1007/BF00170986](https://doi.org/10.1007/BF00170986)
- . 1983, *SoPh*, 88, 179, doi: [10.1007/BF00196186](https://doi.org/10.1007/BF00196186)
- Goddard, C. R., Pascoe, D. J., Anfinogentov, S., & Nakariakov, V. M. 2017, *A&A*, 605, A65, doi: [10.1051/0004-6361/201731023](https://doi.org/10.1051/0004-6361/201731023)
- Goedbloed, H., Keppens, R., & Poedts, S. 2019, *Magnetohydrodynamics of Laboratory and Astrophysical Plasmas* (Cambridge University Press), doi: [10.1017/9781316403679](https://doi.org/10.1017/9781316403679)
- Goossens, M., Erdélyi, R., & Ruderman, M. S. 2011, *SSRv*, 158, 289, doi: [10.1007/s11214-010-9702-7](https://doi.org/10.1007/s11214-010-9702-7)
- Goossens, M., Hollweg, J. V., & Sakurai, T. 1992, *SoPh*, 138, 233, doi: [10.1007/BF00151914](https://doi.org/10.1007/BF00151914)
- Goossens, M., Soler, R., Terradas, J., Van Doorselaere, T., & Verth, G. 2014, *ApJ*, 788, 9, doi: [10.1088/0004-637X/788/1/9](https://doi.org/10.1088/0004-637X/788/1/9)
- Guo, M.-Z., Chen, S.-X., Li, B., Xia, L.-D., & Yu, H. 2016, *SoPh*, 291, 877, doi: [10.1007/s11207-016-0868-3](https://doi.org/10.1007/s11207-016-0868-3)
- Hindman, B. W., & Jain, R. 2021, *ApJ*, 921, 29, doi: [10.3847/1538-4357/ac1a16](https://doi.org/10.3847/1538-4357/ac1a16)
- Hornsey, C., Nakariakov, V. M., & Fludra, A. 2014, *A&A*, 567, A24, doi: [10.1051/0004-6361/201423524](https://doi.org/10.1051/0004-6361/201423524)
- Ionson, J. A. 1978, *ApJ*, 226, 650, doi: [10.1086/156648](https://doi.org/10.1086/156648)
- Jelínek, P., & Karlický, M. 2012, *A&A*, 537, A46, doi: [10.1051/0004-6361/201117883](https://doi.org/10.1051/0004-6361/201117883)
- Karlický, M., Jelínek, P., & Mészáros, H. 2011, *A&A*, 529, A96, doi: [10.1051/0004-6361/201016171](https://doi.org/10.1051/0004-6361/201016171)
- Kolotkov, D. Y., Nakariakov, V. M., Kupriyanova, E. G., Ratcliffe, H., & Shibasaki, K. 2015, *A&A*, 574, A53, doi: [10.1051/0004-6361/201424988](https://doi.org/10.1051/0004-6361/201424988)
- Kolotkov, D. Y., Nakariakov, V. M., Moss, G., & Shellard, P. 2021, *MNRAS*, 505, 3505, doi: [10.1093/mnras/stab1587](https://doi.org/10.1093/mnras/stab1587)
- Kopylova, Y. G., Melnikov, A. V., Stepanov, A. V., Tsap, Y. T., & Goldvarg, T. B. 2007, *Astronomy Letters*, 33, 706, doi: [10.1134/S1063773707100088](https://doi.org/10.1134/S1063773707100088)
- Kupriyanova, E. G., Melnikov, V. F., & Shibasaki, K. 2013, *SoPh*, 284, 559, doi: [10.1007/s11207-012-0141-3](https://doi.org/10.1007/s11207-012-0141-3)
- Li, B., Antolin, P., Guo, M. Z., et al. 2020, *SSRv*, 216, 136, doi: [10.1007/s11214-020-00761-z](https://doi.org/10.1007/s11214-020-00761-z)
- Li, B., Chen, S.-X., & Li, A.-L. 2022, *ApJ*, 928, 33, doi: [10.3847/1538-4357/ac5402](https://doi.org/10.3847/1538-4357/ac5402)
- Li, B., Guo, M., Yu, H., Chen, S.-X., & Shi, M. 2023, *MNRAS*, 518, L57, doi: [10.1093/mnras/1/slac139](https://doi.org/10.1093/mnras/1/slac139)
- Li, B., Guo, M.-Z., Yu, H., & Chen, S.-X. 2018, *ApJ*, 855, 53, doi: [10.3847/1538-4357/aaaf19](https://doi.org/10.3847/1538-4357/aaaf19)
- Lopin, I., & Nagorny, I. 2015a, *ApJ*, 810, 87, doi: [10.1088/0004-637X/810/2/87](https://doi.org/10.1088/0004-637X/810/2/87)
- . 2015b, *ApJ*, 801, 23, doi: [10.1088/0004-637X/801/1/23](https://doi.org/10.1088/0004-637X/801/1/23)
- . 2019, *MNRAS*, 488, 660, doi: [10.1093/mnras/stz1737](https://doi.org/10.1093/mnras/stz1737)
- Mathioudakis, M., Jess, D. B., & Erdélyi, R. 2013, *SSRv*, 175, 1, doi: [10.1007/s11214-012-9944-7](https://doi.org/10.1007/s11214-012-9944-7)
- McLaughlin, J. A., Nakariakov, V. M., Dominique, M., Jelínek, P., & Takasao, S. 2018, *SSRv*, 214, 45, doi: [10.1007/s11214-018-0478-5](https://doi.org/10.1007/s11214-018-0478-5)
- McLean, D. J., & Sheridan, K. V. 1973, *SoPh*, 32, 485, doi: [10.1007/BF00154961](https://doi.org/10.1007/BF00154961)
- Meerson, B. I., Sasorov, P. V., & Stepanov, A. V. 1978, *SoPh*, 58, 165, doi: [10.1007/BF00152562](https://doi.org/10.1007/BF00152562)
- Nakariakov, V. M., Hornsey, C., & Melnikov, V. F. 2012, *ApJ*, 761, 134, doi: [10.1088/0004-637X/761/2/134](https://doi.org/10.1088/0004-637X/761/2/134)
- Nakariakov, V. M., & Kolotkov, D. Y. 2020, *ARA&A*, 58, 441, doi: [10.1146/annurev-astro-032320-042940](https://doi.org/10.1146/annurev-astro-032320-042940)
- Nakariakov, V. M., Melnikov, V. F., & Reznikova, V. E. 2003, *A&A*, 412, L7, doi: [10.1051/0004-6361:20031660](https://doi.org/10.1051/0004-6361:20031660)
- Nakariakov, V. M., & Verwichte, E. 2005, *Living Reviews in Solar Physics*, 2, 3, doi: [10.12942/lrsp-2005-3](https://doi.org/10.12942/lrsp-2005-3)
- Nakariakov, V. M., Pilipenko, V., Heilig, B., et al. 2016, *SSRv*, 200, 75, doi: [10.1007/s11214-015-0233-0](https://doi.org/10.1007/s11214-015-0233-0)
- Nakariakov, V. M., Anfinogentov, S. A., Antolin, P., et al. 2021, *SSRv*, 217, 73, doi: [10.1007/s11214-021-00847-2](https://doi.org/10.1007/s11214-021-00847-2)
- Nechaeva, A., Zimovets, I. V., Nakariakov, V. M., & Goddard, C. R. 2019, *ApJS*, 241, 31, doi: [10.3847/1538-4365/ab0e86](https://doi.org/10.3847/1538-4365/ab0e86)
- Oliver, R., Ruderman, M. S., & Terradas, J. 2014, *ApJ*, 789, 48, doi: [10.1088/0004-637X/789/1/48](https://doi.org/10.1088/0004-637X/789/1/48)

- . 2015, *ApJ*, 806, 56,
doi: [10.1088/0004-637X/806/1/56](https://doi.org/10.1088/0004-637X/806/1/56)
- Oliver, R., Soler, R., Terradas, J., & Zaqarashvili, T. V. 2016, *ApJ*, 818, 128,
doi: [10.3847/0004-637X/818/2/128](https://doi.org/10.3847/0004-637X/818/2/128)
- Parks, G. K., & Winckler, J. R. 1969, *ApJL*, 155, L117, doi: [10.1086/180315](https://doi.org/10.1086/180315)
- Pascoe, D. J., Goddard, C. R., Anfinogentov, S., & Nakariakov, V. M. 2017, *A&A*, 600, L7,
doi: [10.1051/0004-6361/201730458](https://doi.org/10.1051/0004-6361/201730458)
- Poedts, S., & Kerner, W. 1991, *PhRvL*, 66, 2871,
doi: [10.1103/PhysRevLett.66.2871](https://doi.org/10.1103/PhysRevLett.66.2871)
- Roberts, B. 2000, *SoPh*, 193, 139,
doi: [10.1023/A:1005237109398](https://doi.org/10.1023/A:1005237109398)
- Roberts, B. 2019, *MHD Waves in the Solar Atmosphere* (Cambridge University Press),
doi: [10.1017/9781108613774](https://doi.org/10.1017/9781108613774)
- Roberts, B., Edwin, P. M., & Benz, A. O. 1983, *Nature*, 305, 688, doi: [10.1038/305688a0](https://doi.org/10.1038/305688a0)
- . 1984, *ApJ*, 279, 857, doi: [10.1086/161956](https://doi.org/10.1086/161956)
- Rosenberg, H. 1970, *A&A*, 9, 159
- Schrijver, C. J. 2007, *ApJL*, 662, L119,
doi: [10.1086/519455](https://doi.org/10.1086/519455)
- Sewell, G. 1988, *The Numerical Solution of Ordinary and Partial Differential Equations* (San Diego: Academic Press)
- Soler, R., & Goossens, M. 2011, *A&A*, 531, A167,
doi: [10.1051/0004-6361/201116536](https://doi.org/10.1051/0004-6361/201116536)
- Soler, R., Goossens, M., Terradas, J., & Oliver, R. 2013, *ApJ*, 777, 158,
doi: [10.1088/0004-637X/777/2/158](https://doi.org/10.1088/0004-637X/777/2/158)
- Soler, R., & Terradas, J. 2015, *ApJ*, 803, 43,
doi: [10.1088/0004-637X/803/1/43](https://doi.org/10.1088/0004-637X/803/1/43)
- Spruit, H. C. 1982, *SoPh*, 75, 3,
doi: [10.1007/BF00153456](https://doi.org/10.1007/BF00153456)
- Terradas, J., Andries, J., & Goossens, M. 2007, *SoPh*, 246, 231,
doi: [10.1007/s11207-007-9067-6](https://doi.org/10.1007/s11207-007-9067-6)
- Terradas, J., Oliver, R., & Ballester, J. L. 2005a, *ApJL*, 618, L149, doi: [10.1086/427844](https://doi.org/10.1086/427844)
- . 2005b, *A&A*, 441, 371,
doi: [10.1051/0004-6361:20053198](https://doi.org/10.1051/0004-6361:20053198)
- . 2006, *ApJ*, 642, 533, doi: [10.1086/500730](https://doi.org/10.1086/500730)
- Terradas, J., Soler, R., Oliver, R., et al. 2022, *A&A*, 660, A136,
doi: [10.1051/0004-6361/202142975](https://doi.org/10.1051/0004-6361/202142975)
- Uchida, Y. 1970, *PASJ*, 22, 341
- Van Doorselaere, T., Kupriyanova, E. G., & Yuan, D. 2016, *SoPh*, 291, 3143,
doi: [10.1007/s11207-016-0977-z](https://doi.org/10.1007/s11207-016-0977-z)
- Vasheghani Farahani, S., Hornsey, C., Van Doorselaere, T., & Goossens, M. 2014, *ApJ*, 781, 92, doi: [10.1088/0004-637X/781/2/92](https://doi.org/10.1088/0004-637X/781/2/92)
- Verwichte, E., Nakariakov, V. M., & Cooper, F. C. 2005, *A&A*, 430, L65,
doi: [10.1051/0004-6361:200400133](https://doi.org/10.1051/0004-6361:200400133)
- Wentzel, D. G. 1979, *ApJ*, 227, 319,
doi: [10.1086/156732](https://doi.org/10.1086/156732)
- Yu, H., Li, B., Chen, S., & Guo, M. 2021, *SoPh*, 296, 95, doi: [10.1007/s11207-021-01839-9](https://doi.org/10.1007/s11207-021-01839-9)
- Yu, H., Li, B., Chen, S.-X., & Guo, M.-Z. 2015, *ApJ*, 814, 60,
doi: [10.1088/0004-637X/814/1/60](https://doi.org/10.1088/0004-637X/814/1/60)
- Yu, H., Li, B., Chen, S.-X., Xiong, M., & Guo, M.-Z. 2017, *ApJ*, 836, 1,
doi: [10.3847/1538-4357/836/1/1](https://doi.org/10.3847/1538-4357/836/1/1)
- Zajtsev, V. V., & Stepanov, A. V. 1975, *Issledovaniia Geomagnetizmu Aeronomii i Fizike Solntsa*, 37, 3
- Zimovets, I. V., & Nakariakov, V. M. 2015, *A&A*, 577, A4, doi: [10.1051/0004-6361/201424960](https://doi.org/10.1051/0004-6361/201424960)
- Zimovets, I. V., McLaughlin, J. A., Srivastava, A. K., et al. 2021, *SSRv*, 217, 66,
doi: [10.1007/s11214-021-00840-9](https://doi.org/10.1007/s11214-021-00840-9)

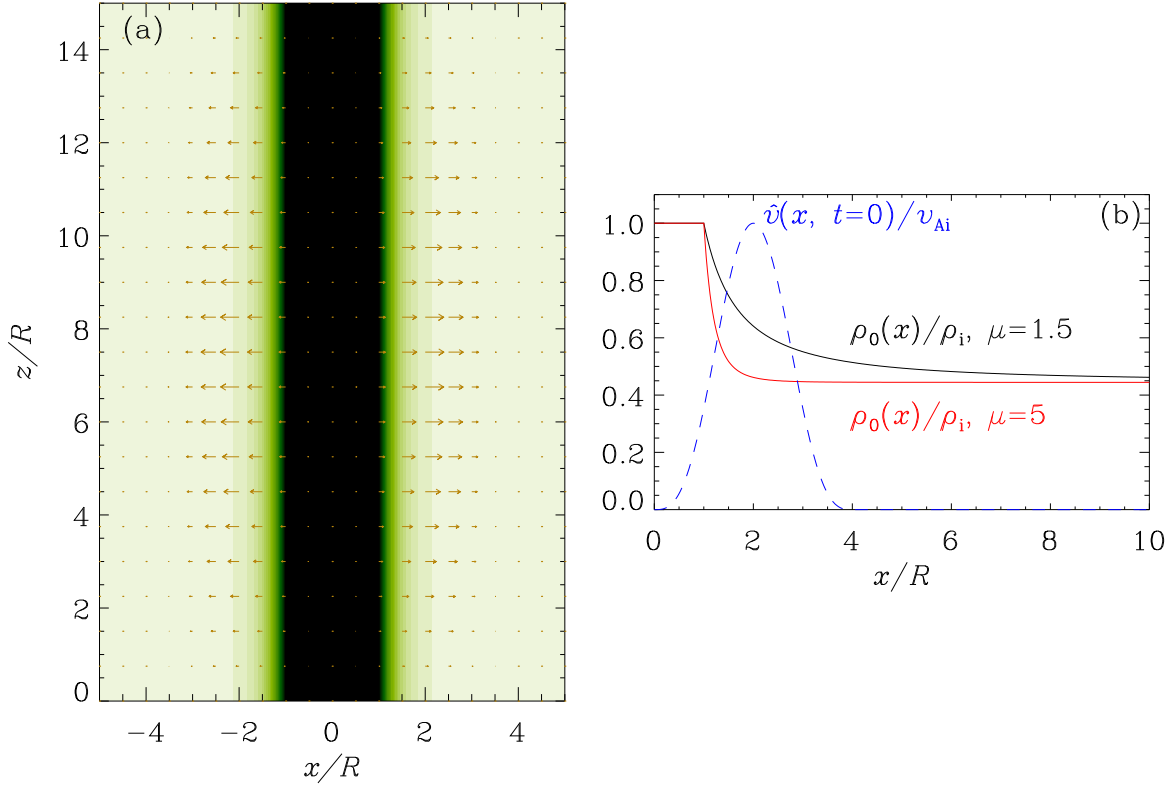


Figure 1. (a) Two-dimensional (2D) representation of the 1D initial value problem (IVP 1). Plotted are the $x - z$ distributions of the equilibrium density (the filled contours) and the initial velocity field (the arrows). The examined slabs possess a nominal half-width R . Axial fundamentals are ensured by the z -dependence of the initial perturbation. (b) Illustrative transverse profiles of the initial perturbation (\hat{v} , the blue dashed curve) and the equilibrium density (ρ_0 , the solid curves), both involved in IVP 1. The density profile follows the outer μ prescription in Equation (1), with the density contrast ρ_i/ρ_e chosen to be 2.25. Two steepness parameters are plotted, namely $\mu = 1.5$ (the black curve) and $\mu = 5$ (red). The initial perturbation is described by Equation (8), with the spatial extent Λ chosen to be $4R$ here.

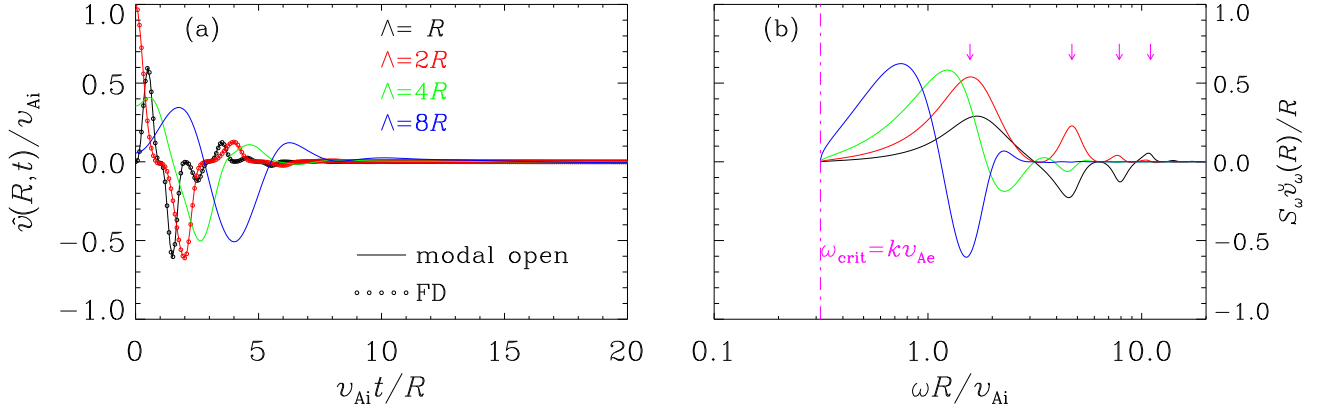


Figure 2. “Modal Open” solutions to IVP 1 for a coronal slab with step density profile ($\mu = \infty$) and a density contrast of $\rho_i/\rho_e = 2.25$. The dimensionless axial wavenumber is fixed at $kR = \pi/15$. By “Modal Open” we mean that the solution is constructed by superposing the eigenmodes for an open system. A number of values are examined for the spatial extent (Λ) of the initial perturbation as discriminated by the different colors. Plotted in (a) are the temporal profiles of the transverse speed at the nominal slab half-width, namely $\hat{v}(R, t)$. In addition to the “Modal Open” solutions (the solid curves), the finite-difference solutions are also presented for two values of Λ for comparison (the black and red symbols). Presented in (b) are the frequency dependencies of the local spectral densities at the nominal slab half-width, namely $S_{\omega} \check{v}_{\omega}(R)$. The vertical dash-dotted line represents the critical frequency $\omega_{crit} = kv_{Ae}$. The real parts of the mode frequencies for the first several discrete leaky modes (DLMs) are indicated by the magenta arrows. These DLMs are computed with Equation (37), the dispersion relation (DR) pertaining to an eigenvalue problem (EVP) that does not allow incoming waves at infinity. The continuous curves, however, derive from the improper continuum that results from an EVP for which no boundary condition is specified at infinity. See text for more details.

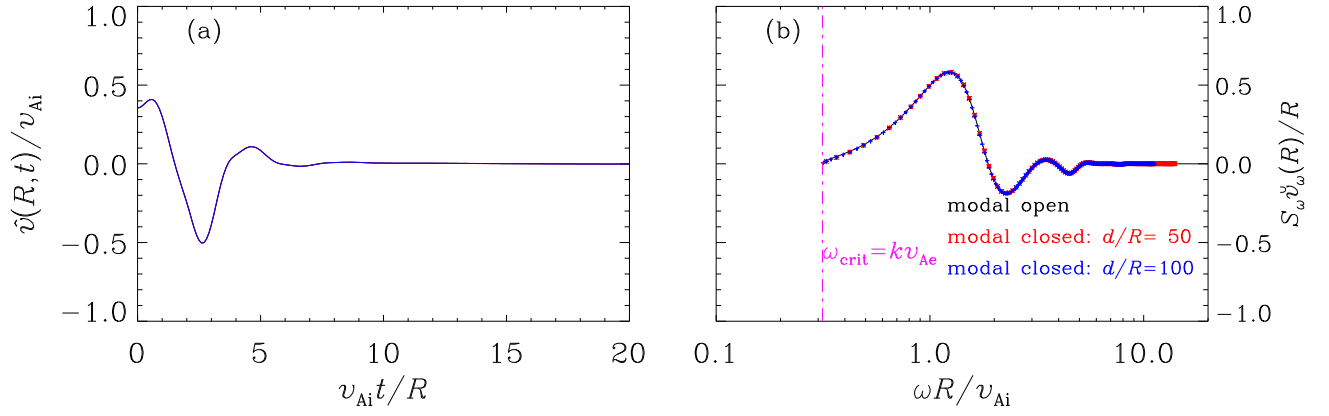


Figure 3. Similar to Figure 2 but for a fixed combination $[\rho_i/\rho_e, kR, \Lambda/R] = [2.25, \pi/15, 4]$. The “Modal Open” solution is represented by the black curves in both (a) and (b). Additional “Modal Closed” solutions are presented as found by superposing the eigenmodes for the EVP defined on closed domains (EVP 1). Two domain sizes are discriminated by the different colors, one being $d/R = 50$ and the other being $d/R = 100$. The eigenfrequencies for EVP 1 are discrete by construction. See text for more details.

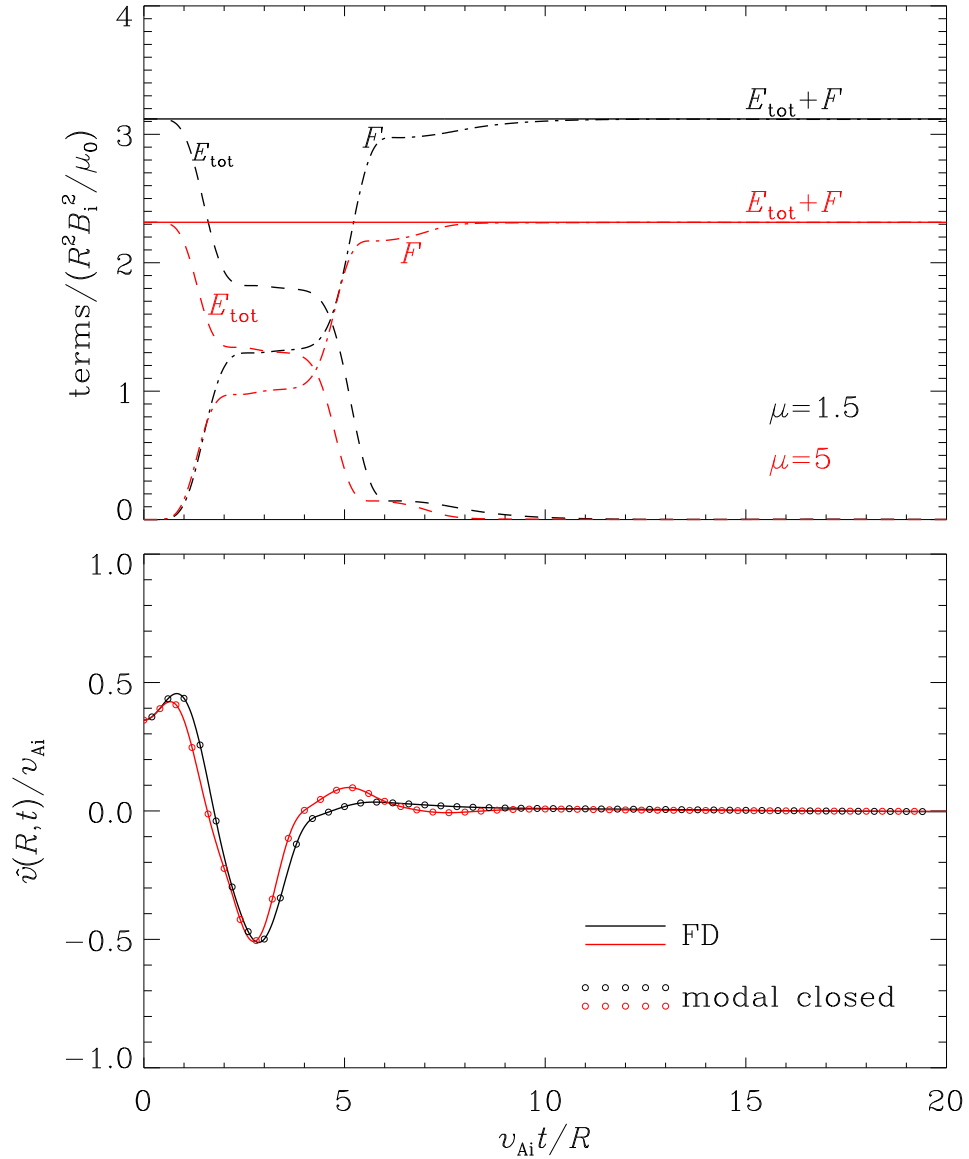


Figure 4. FD solutions to IVP 1 for two steepness parameters, one being $\mu = 1.5$ (the black curves) and the other being $\mu = 5$ (red), given a fixed combination $[\rho_i/\rho_e, kR, \Lambda/R] = [2.25, \pi/15, 4]$. Plotted in (a) are the terms characterizing the energy content in the volume \mathcal{V} where the initial perturbation is applied, with E_{tot} and F representing the total wave energy in and the cumulative energy loss from \mathcal{V} (see Equations (10) to (12)). The transverse speeds at the nominal half-width $\hat{v}(R, t)$ are shown against time in (b), where the “Modal Closed” solutions are presented by the symbols as labeled. These solutions are obtained with Equation (23), with the domain size chosen to be $d = 50 R$.

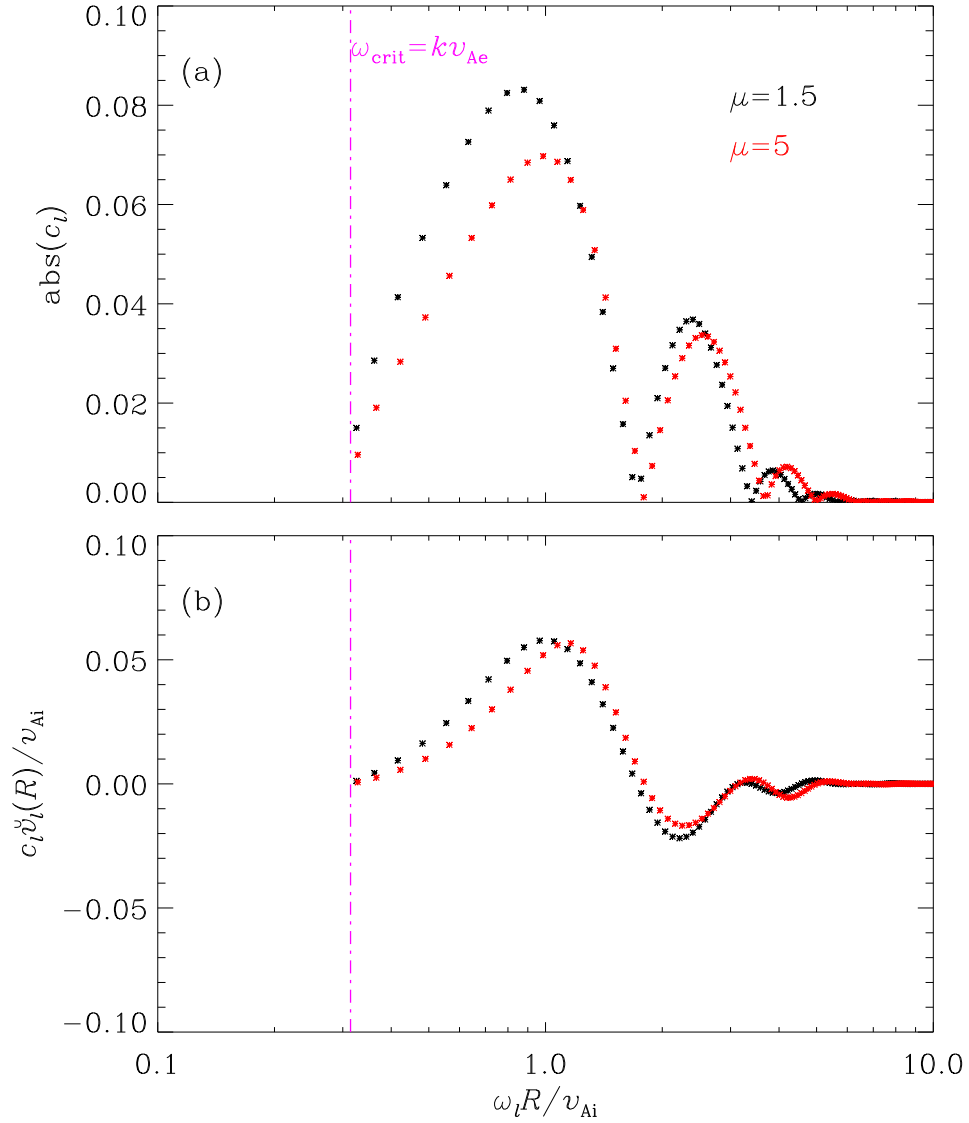


Figure 5. Frequency-dependencies of the contributions of individual modes for a fixed combination $[\rho_i/\rho_e, kR, \Lambda/R, d/R] = [2.25, \pi/15, 4, 50]$. Two steepness parameters, $\mu = 1.5$ and $\mu = 5$, are examined as labeled. The sets of position-independent coefficients $\{c_l\}$ are plotted in (a), while the specific contributions at the half-width $c_l \check{v}_l(R)$ are presented in (b). The critical frequency $\omega_{\text{crit}} = k v_{Ae}$ is represented by the vertical dash-dotted lines for reference.

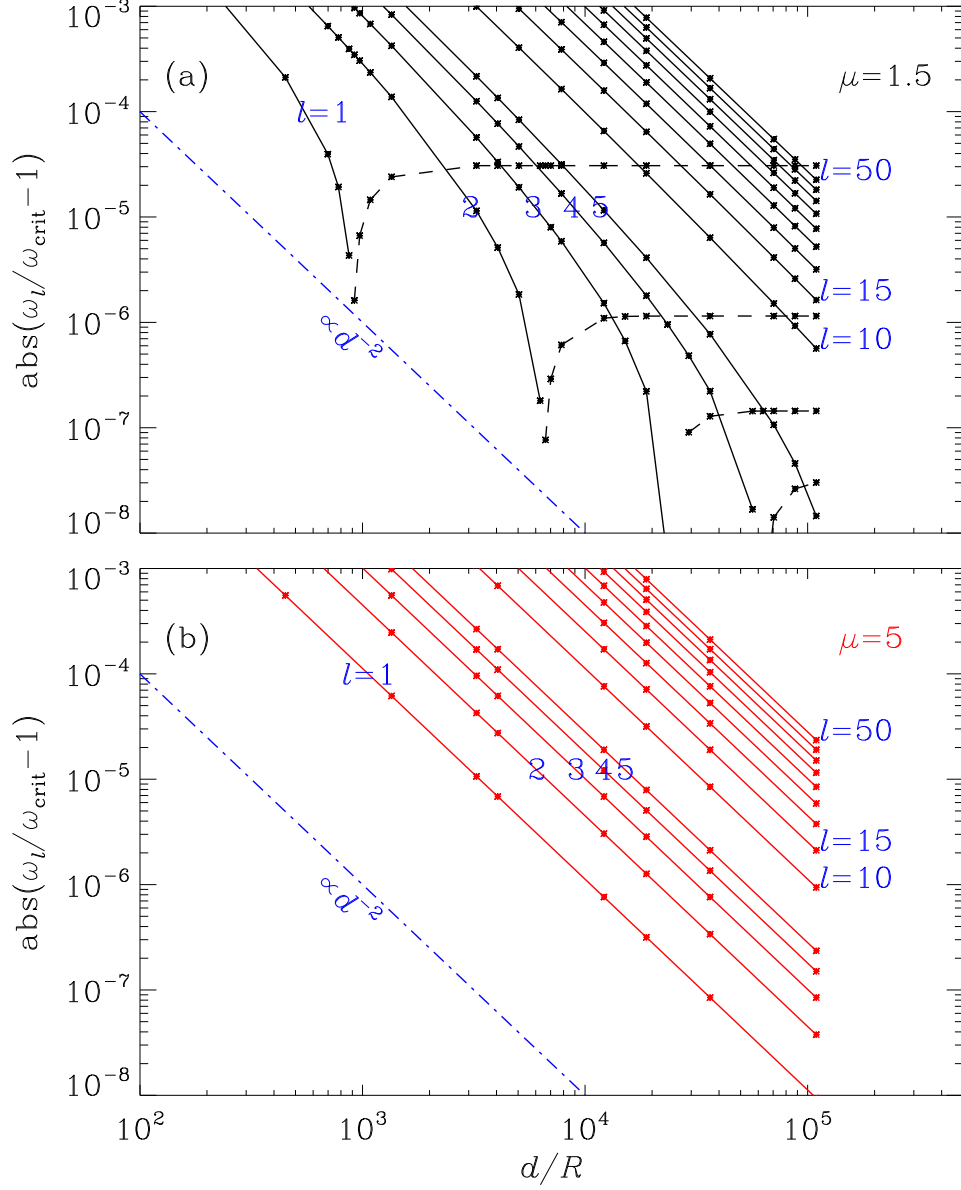


Figure 6. Dependencies of the modulus of the fractional difference $\delta_l = \omega_l/\omega_{\text{crit}} - 1$ on the dimensionless domain size (d/R) for two steepness parameters, (a) $\mu = 1.5$ and (b) $\mu = 5$, given a combination $[\rho_i/\rho_e, kR] = [2.25, \pi/15]$. For each pair $[\mu, d/R]$, the first five eigenmodes are always presented, while the rest are uniformly sampled in l with a step of five when l lies in the range between 10 and 50. A solid (dashed) curve is employed to connect $|\delta_l|$ for a given l when δ_l is positive (negative). The blue dash-dotted lines represent the $1/d^2$ -dependence for comparison. See text for more details.

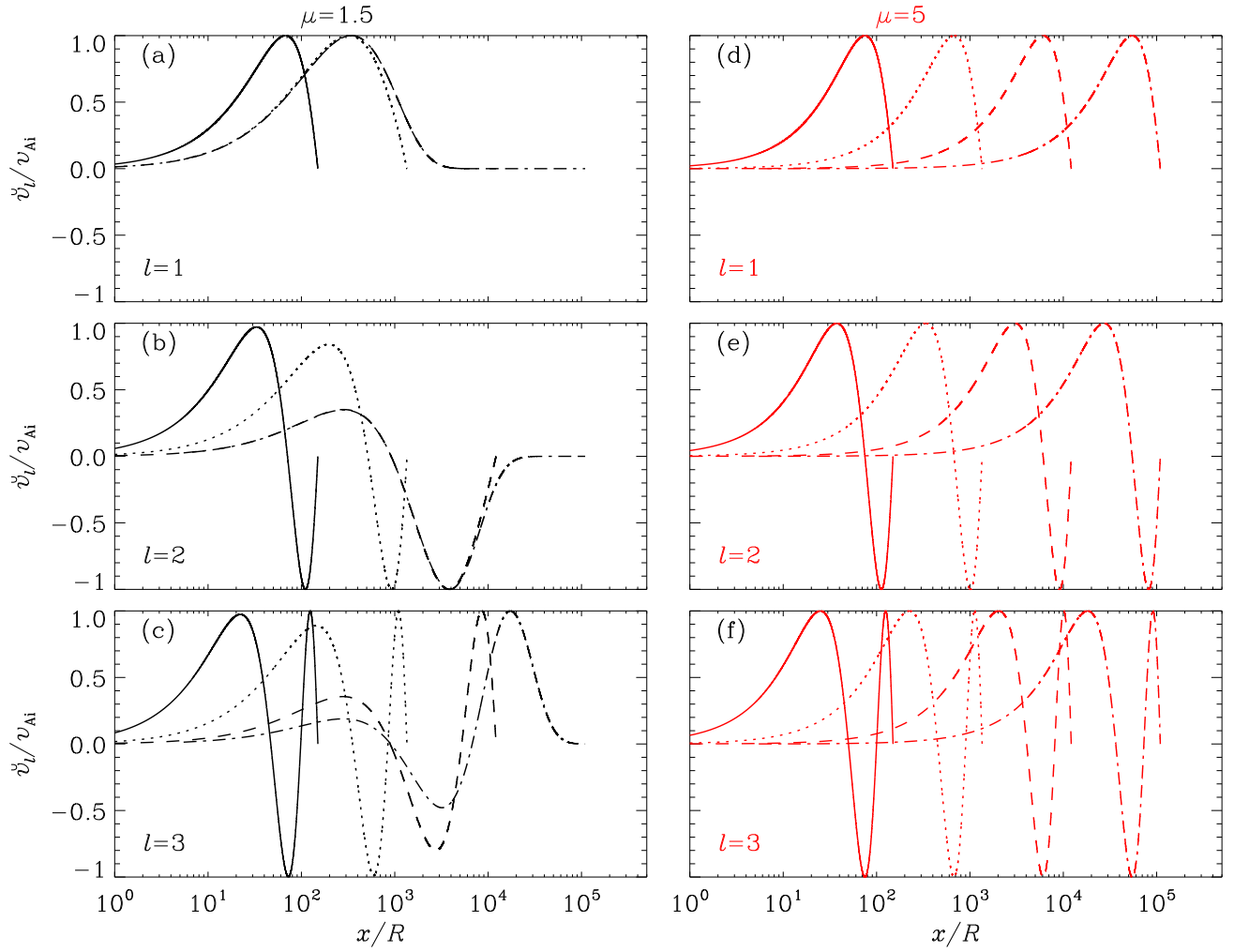


Figure 7. First three eigenfunctions for EVP 1 on a number of domains differentiated by the linestyles, given a fixed combination $[\rho_i/\rho_e, kR] = [2.25, \pi/15]$. Two steepness parameters are examined, one being $\mu = 1.5$ (the left column) and the other being $\mu = 5$ (right). The eigenfunctions are arbitrarily scaled such that their dependencies on the domain size can be better visualized. See text for more details.

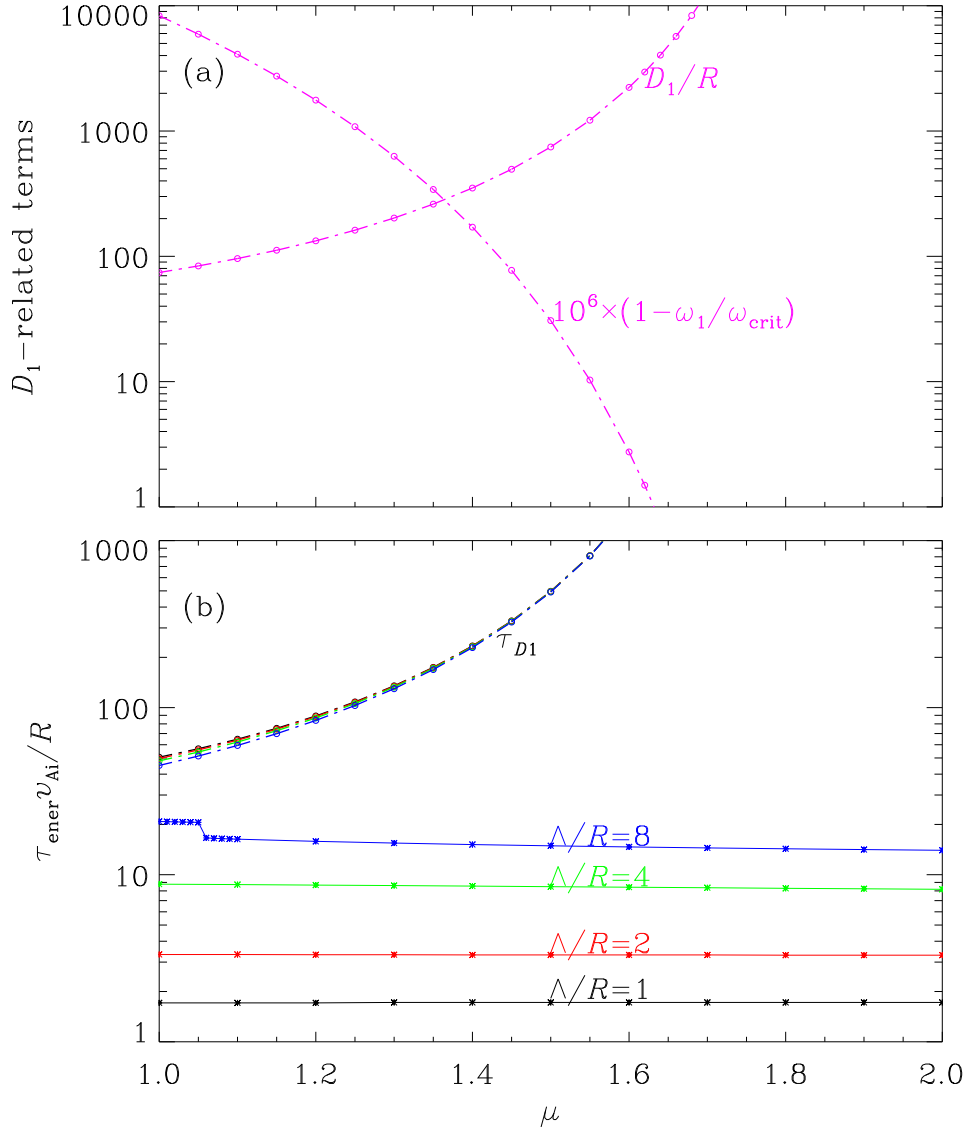


Figure 8. Some scales characterizing the solutions to EVP 1 and IVP 1 for a fixed pair $[\rho_i/\rho_e, kR] = [2.25, \pi/15]$. Plotted in (a) is the μ -dependence of D_1 , the distance beyond which the first eigenfunction is evanescent. The fractional difference $1 - \omega_1/\omega_{\text{crit}}$ is also displayed for reference. Panel (b) presents, by the solid curves, the variations of some timescale τ_{ener} against μ for a number of Λ as determined from the FD solutions to IVP 1. Here τ_{ener} denotes the time at which the total energy drops by a factor of $e^4 \approx 55$ relative to its initial value in the volume where the initial perturbation is applied. The dash-dotted curves represent the μ -dependencies of another Λ -related timescale τ_{D1} , the time when the position $x = D_1$ is disturbed. The curves for both τ_{ener} and τ_{D1} are color-coded by the values of Λ . See text for more details.